DEGREE PROJECT

Insights into the burning behaviour of wood in the cone calorimeter

Ellinor Sanned

Fire Engineering, master's level
2022

Luleå University of Technology
Department of Civil, Environmental and Natural Resources Engineering

LULEÅ UNIVERSITY OF TECHNOLOGY

Title	Insights into the burning behaviour of wood in the cone calorimeter
Titel	Studier om förbränningsförloppet av trä i konkalorimetern
Author	Ellinor Sanned Master Programme in Fire Engineering
Main supervisor	Rhoda Afriyie Mensah Luleå University of Technology, Division of Structural and Fire Engineering
Second supervisor	Oisik Das Luleå University of Technology, Division of Structural and Fire Engineering
Examiner	Michael Försth Luleå University of Technology, Division of Structural and Fire Engineering
Keywords	Wood combustion, fire test, cone calorimetry, heat release rate, char formation
Sökord	Träförbränning, brandtest, konkalorimetri, värmeavgivnings-hastighet, förkolning

Preface and Acknowledgments

This study is my master's thesis for the Master Programme in Fire Engineering at Luleå University of Technology. The course corresponds to 30 higher education credits and has been completed during the spring of 2022.

I hope that the study will contribute to a deeper understanding of the burning behaviour of wood and that it will provide new questions for further research in the area.

I would like to thank my supervisor Rhoda Afriyie Mensah who has helped me perform my laboratory work and structure my thesis. I would also like to thank my second supervisor Oisik Das who has been a great support in analysing the SEM-data and answering questions regarding the results. Moreover, I would like to thank my examiner Michael Försth for answering questions and participating in discussions concerning the work.

Finally, I want to thank my family, thank you for all the support and encouragement you have given me throughout the working process.

Ellinor Sanned

Jönköping, June 2022

Abstract

Climate change and its accompanying environmental issues have caused the building industry to use more environmentally friendly building materials. Wood have always been a building material but due to the renewed interest in imparting sustainability and renewability, its usage has increased over the recent years. With a rising interest in wood, it is of great importance to enhance the knowledge of its burning behaviour in order to predict and prevent fire hazards. Fire development is often characterized in terms of heat release rate (HRR) as a function of time. Therefore, HRR is considered one of the most important variables in the evaluation of material fire hazards.

This study aims to generate greater knowledge of the HRR curve of wood when exposed to heating in the cone calorimeter and how the curve can be described quantitatively. Furthermore, it was attempted to comprehend the properties and functions of char and its effects on HRR during combustion.

The study is based on laboratory tests carried out with a cone calorimeter and a Scanning Electron Microscope (SEM). The cone calorimeter was set to generate a heat flux of 35 kWm^{-2}. Spruce wood samples of three thicknesses were analysed, namely 10, 20 and 30 mm. The samples were assembled with one of three types of material on the rear side of the samples, which were Kaowool, steel plates and aluminium foil wrapped around wood. The different materials were used as they are greatly dissimilar in their thermal properties. Wood with both low and normal moisture content was also analysed. Char was analysed with SEM.

The results show that there are four major points of interest in the HRR curve of wood. The first point is the initial peak heat release rate (PHRR) that occurs when the sample surface ignites causing great production of heat which increases the HRR. The second point of interest is the vast decrease in HRR soon after the first PHRR, this is due to char formation, which acts as a protective barrier preventing the exchange of volatile gases and oxygen. The third point of interest is a second PHRR close to the end of the combustion that occurs as a response to sample burn through, which means that the heat gradient reaches the rear side of the sample. The second PHRR is highly dependent on the boundary condition defined by the rear material, which determines the heat losses at the rear side of the specimen, and consequently the temperature of the specimen. The higher is the specimen temperature, the higher is the pyrolysis rate, and therefore also the higher the second PHRR. Moreover, high moisture content delays the time of occurrence of the second PHRR as more water needs to undergo phase change, which requires a high amount of energy. The final point of interest is the final decrease in HRR as a result of fuel depletion leading to the sample smouldering or the fire being extinguished.

Char, formed by mainly lignin and some cellulose in wood, affects the overall HRR. The SEM analysis showed that the char cracks grew wider during the second PHRR. It is, however, observed that char cracking has no significance in the time of occurrence of the second PHRR as this is based on sample burn through, and it was difficult to determine to what extent char cracking affected the intensity of the PHRR.

This systematic study is considered adequate to justify the research questions and aim of this study. It has also created new questions for further study in the area as well as provided a deeper understanding of the fundamental burning behaviour of wood.

Sammanfattning

Klimatförändringen och dess medföljande miljöfrågor har fått byggbranschen att använda mer hållbara och miljövänliga byggmaterial. Trä har alltid varit ett byggmaterial men på grund av ett förnyat intresse för hållbarhet och förnybarhet har användningen av materialet ökat under de senaste åren. Med ett stigande intresse för trä är det av stor vikt att öka kunskapen om dess förbränningsbeteende för att kunna förutse och förebygga brandrisker. Brandutveckling karakteriseras ofta i termer av värmeavgivningshastighet (HRR) som funktion av tid. Det är därför en av de viktigaste variablerna i utvärderingen av brandrisker.

Denna studie syftar till att skapa större kunskap om HRR-kurvan för trä när det utsätts för värme i konkalorimetern och hur kurvan kan beskrivas kvantitativt. Vidare, att studera kollagrets egenskaper och funktioner samt hur det påverkar HRR under förbränning.

Studien bygger på laborativa försök utförda med en konkalorimeter och ett svepelektronmikroskop (SEM). Konkalorimetern genererade strålning med intensitet 35 kWm^{-2}. Tre tjocklekar av granprover testades, 10, 20 och 30 mm. Proverna placerades ovanpå en av tre typer av material i en provform, Kaowool, stålplattor och trä invirat i aluminiumfolie. Materialen användes då deras termiska egenskaper skiljer sig åt. Vidare testades även trä av både låg och normal fukthalt. Kollagret analyserades med SEM.

Resultatet visar att det finns fyra intressanta områden på HRR-kurvan för trä. Det första är den initiala maximala värmeavgivningshastigheten (PHRR) som inträffar när provytan antänder vilket orsakar en stor värmeproduktion som ökar HRR. Det andra är en kraftig minskning av HRR strax efter den första PHRR. Detta beror på att kol börjat bildas på provytan, kollagret fungerar som en skyddande barriär som förhindrar utbyte av flyktiga gaser och syre. Det tredje är en andra PHRR som inträffar nära brandprovets slut. Detta sker till följd av provkroppsgenombränning som innebär att värmegradienten når provets baksida. Intensiteten av PHRR är starkt beroende av materialet bakom provet. Det bestämmer värmeförlusten på provets baksida och därmed även provkroppens temperatur. Ju högre provkroppstemperaturen är, desto högre är pyrolyshastigheten vilket leder till en högre andra PHRR. Hög fukthalt fördröjer även tidpunkten för uppkomsten av den andra PHRR eftersom fasomvandling av vatten kräver en stor mängd energi. Det sista och fjärde området av intresse är en minskning av HRR efter den andra PHRR, detta sker när allt bränsle förbränts och det som kvarstår är endast ett glödande prov.

Kollagret, som främst bildas av lignin och en del cellulosa i träet, påverkar den totala HRR. SEM-analysen visade att sprickorna i kollagret blev bredare under den andra PHRR. Däremot observerades det att sprickbildningen inte har någon betydelse för tidpunkten av den andra PHRR uppkomst då denna enbart är baserad på provets genombränning. Det är även svårt att avgöra i vilken utsträckning sprickbildningen påverkar intensiteten av PHRR.

Metoden som används för att besvara frågeställningarna och syftet anses vara adekvat. Studien har öppnat upp för ytterligare frågeställningar och idéer till fortsatta försök inom området. Vidare har även studien gett en djupare förståelse om förbränningsbeteendet av trä.

Table of content

Nomenclature

Legend

$\dot{Q}$	Heat release rate	[kWm^{-2}]*
$\dot{m}$	Mass loss rate	[kgm^{-2}s^{-1}]
ΔH_{eff}	Effective heat of combustion	[kJkg^{-1}]
$\Delta \eta_{O_2}$	Mole fraction of oxygen	[-]
$\dot{V}$	Volumetric flow	[m^{3}s^{-1}]
ρ_{O_2}	Density of oxygen	[kgm^{-3}]

Abbreviations

HRR	Heat release rate
PHRR	Peak heat release rate
THR	Total heat release
MLR	Mass loss rate
RH	Relative humidity
T/C	Thermocouple
PT	Plate thermometer

* Equation 1 and 2 calculates $\dot{Q}$ [kW]

1 Introduction

The following section presents the background as well as the purpose, research questions and boundaries.

1.1 Background

Timber has been in use for centuries and is one of the world's oldest construction materials. Timber construction has always had a strong economic and social value, and today it is used throughout the world (Khatib, 2016).

As climate change becomes increasingly critical it has been pivotal to consider and produce sustainable building materials. Therefore, the environmental significance of wood as a natural resource with renewable and sustainable properties has become more important than ever (Khatib, 2016).

As timber receives more attention as a construction material it is important to understand its combustion properties as well as enhance the understanding of its behaviour when exposed to fire. Furthermore, different substrates commonly affixed to the wooden structure (e.g., insulation) have varying thermal properties, which govern the sustained burning behaviour of the structure, depending on the thickness. Hence, understanding the relationship of the reaction-to-fire properties of wood having varying thicknesses with its substrate is critical to ensure fire-safety in buildings. This knowledge is useful both in production and when preventing fire hazards or possible pollution from combustion.

Heat release rate (HRR), $\dot{Q}$, also called energy release rate, indicates the amount of released energy per unit time for a given burning object and for most materials it changes over time. Studying energy released in a compartment fire gives insight into fire properties such as hot gas temperatures, plume flows and rate of descent of hot gas layers. Hence, fire development is often characterized in terms of HRR versus time (Karlsson & Quintiere, 1999) making HRR one of the most important variables when it comes to evaluating material fire hazards (Fateh et al., 2014). Over time the HRR curves of materials with thick charring, such as wood, tend to peak at the start where no charring has yet occurred as well as at the end of the combustion cycle, see Figure 1. According to Schartel and Hull (2007), the second peak is believed to be a response to an increase in the effective pyrolysis or by cracking char, however these reasons are not verified.

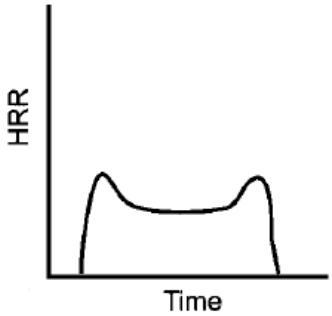

Figure 1. Heat release rate of wood (Schartel & Hull, 2007), reproduced with permission.

Moreover, Tran (1992) argues that the first peak in wood HRR is a result of the burning of the pyrolysis zone soon after ignition. The decrease in HRR is due to the char acting as insulation, meaning that if the wood sample is sufficiently thick, the second HRR peak will not occur. The second peak occurs when the burning is near the rear side of the sample and the bulk temperature of the remnant material is quickly raised.

It is clear that the reason for the appearance of the HRR curve of wood is not determined experimentally and many assumptions have been made, especially regarding the second peak of the HRR curve. Therefore, it is both valuable and interesting to do a thorough analysis of the HRR curve of wood since it is a crucial factor to characterise fire.

1.1.1 Problem description

According to Forest Products Laboratory (2013) wood has become an increasingly important topic as the material possesses environmental benefits that few others do, e.g. low carbon impact, low embodied energy (the amount of energy required to harvest, manufacture and transport a material) and sustainability. The material is suitable for multiple different applications and has therefore become one of the most commonly used construction materials. It is used in a wide range of applications, from small houses to large, complex, and highly engineered buildings. The building industry strives to utilise a sustainable approach to produce raw materials, thus making wood very attractive since one of its greatest attributes is being a renewable resource. As a result, by following sustainable harvesting practices and forest management, wood will be available for an indefinite period (Forest Products Laboratory, 2013).

Fire safety is of great importance in the building industry leading to high demands on design requirements and limitations in construction codes. To fully understand the fire and burning behaviour of wood it has been studied for a long time, making its fire-performance characteristics (thermal degradation, ignition, smoke and heat release, charring rate and flame spread), well documented (Forest Products Laboratory, 2013). However, there is a dearth of literature on the phenomena that affect the various stages of HRR, especially the second peak, as most commonly observed in a cone calorimeter. As HRR is one of the most important variables in the evaluation of material fire hazards (Fateh et al., 2014), it is of great importance to study and gain a deeper understanding of its complexity. A better understanding of the combustion and decomposition process of wood gives knowledge that can be useful in both production and research, and perhaps to enhance fire protection properties.

1.2 Purpose

The purpose of this thesis is to shed light on the various stages of the HRR curve of wood when exposed to radiative heating in a cone calorimeter.

1.2.1 Research questions

The research questions of this study are:

- How can the different stages of the HRR curve of wood be described quantitatively?
- How important is the char layer and its properties/functions during combustion and how does it affect the HRR?

1.3 Boundaries

This study was limited to only concern cone calorimeter tests with heat flux set to 35 kWm^{-2}. The tested sample specimens were of spruce wood with area 100x100 mm and thicknesses of 10, 20 and 30 mm. Each test was replicated with a minimum of three times.

2 Method

The following sections present the methodology, the approach to collecting data, an explanation of the instruments used in the laboratory work and the execution of the laboratory tests.

2.1 Methodology

The study is an explicative enquiry where deeper understanding of the field in question is required. The study is based on literature studies and experimentally performed laboratory work (Björklund & Paulsson, 2016). The literature study provides background on previous research and the laboratory work was performed with a cone calorimeter from Fire Testing Technology (FTT) and a Scanning Electron Microscope (SEM) available at Luleå University of Technology.

The process began with identifying problems and issues regarding the HRR of wood through a literature review. In consultation with supervisors Rhoda Afriyie Mensah, Oisik Das and examiner Michael Försth it was decided to perform laboratory work to further study the subject. Subsequently, analysis of the result together with literature reviews created a final compilation. Figure 2 illustrates a visualization of the approach of the chosen method.

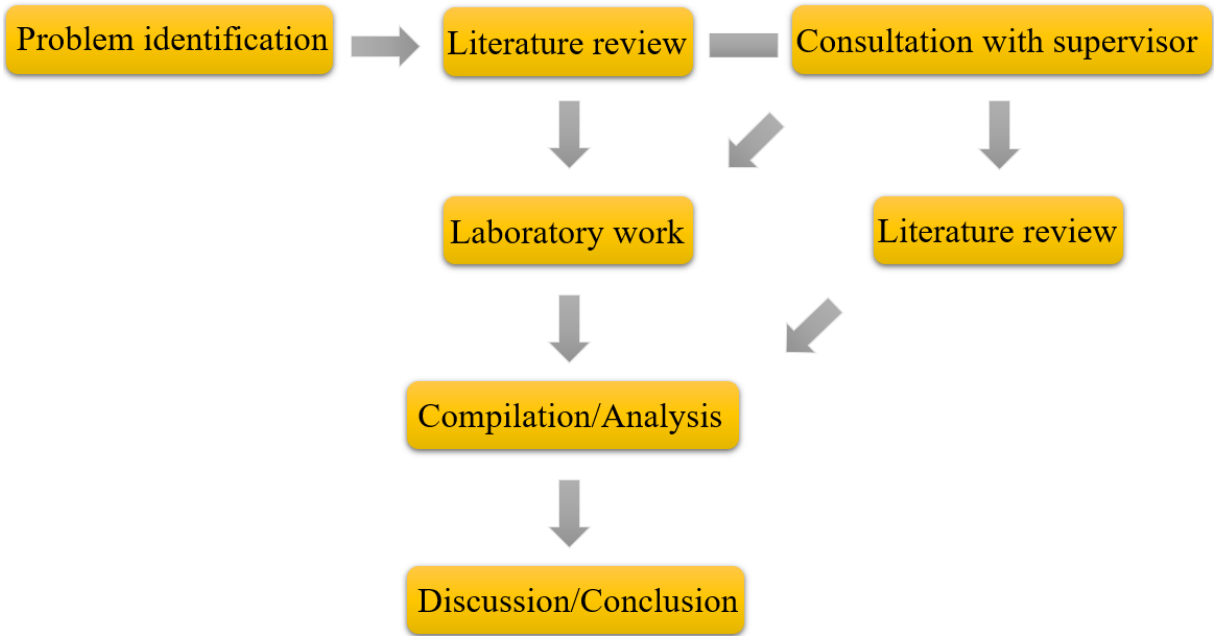

Figure 2. Visualisation of the methodology (Björklund & Paulsson, 2016).

2.2 Data collection

Two methods of data collection were used, these were literature study and laboratory tests. Below is a description of each method.

2.2.1 Literature study

A literature study was performed to collect information from existing research performed on the HRR of wood. It created an understanding of the problems and research questions in this field. Furthermore, a clarification of the significance of the research was made.

The literature provided an understanding of the cone calorimeter and Scanning Electron Microscope (SEM), which made it possible to prepare the laboratory tests. Moreover, the gained knowledge made it possible to analyse and interpret the results.

2.2.2 Laboratory tests

Multiple articles and papers on cone calorimeter tests similar to the ones in this thesis were studied to create an idea of which temperature and heat flux (thermal radiation) intensity that were suitable for the laboratory work. The used heat fluxes vary from 30-75 kWm^{-2} where the higher the heat flux the shorter the ignition and measurement time (Schartel & Hull, 2007). A smaller intensity of heat flux is more suitable for this study as the results are generated more moderately and therefore it is easier to analyse the burning and decomposition process. Hence, the chosen heat flux was 35 kWm^{-2}.

Laboratory work was performed on spruce wood (soft-wood) of three different thicknesses - 10, 20 and 30 mm. This gave an insight into the effect of thickness on HRR. To identify the significance an insulation has on HRR three types of materials were used on the rear side of the sample during the experiment. These were kaowool (insulation that provides low heat loss), steel (providing high heat loss) and aluminium foil wrapped around wood (no more combustion but the same thermal properties as the tested wood). Moreover, fragments/bits from both pristine wood, char and ash were analysed with SEM to identify the effects of char on the HRR. Additional measurements of temperature and relative humidity was carried out to analyse the temperature gradient and moisture transport at the bottom of the sample and their effect on the HRR.

A further description of the performed laboratory work is presented in section 2.7.

2.3 Cone calorimeter

It was thought in the 1970s that the best way to measure and determine fire properties of different materials was through their HRR. Hence, in 1982 the cone calorimeter, created by the fire department at National Institute of Standards and Technology (NIST), was introduced and has since then been acknowledged as the most important bench scale instrument when it comes to fire testing (National Institute of Standards and Technology [NIST], 2021). The apparatus exposes a sample to a specific heat flux, and subsequently it can measure and analyse the combustion gases and smoke. HRR is proportional to oxygen consumed during combustion by a material and is described as the materials mass loss rate (MLR) multiplied by the effective heat of combustion, according to Equation 1.

$$\dot{Q} = \dot{m} \cdot \Delta H_{eff} \tag{1}$$

where $\dot{Q}$ is HRR [kW], $\dot{m}$ is MLR [kgs^{-1}] and ΔH_{eff} is the effective heat of combustion [$kJkg^{-1}$] (Karlsson & Quintiere, 2000).

The cone calorimeter is equipped with multiple parts, see Figure 3, that work together to set, adjust, log, and measure different parameters such as mass, temperature, gas flow and gas concentration (Lindholm et al., 2009).

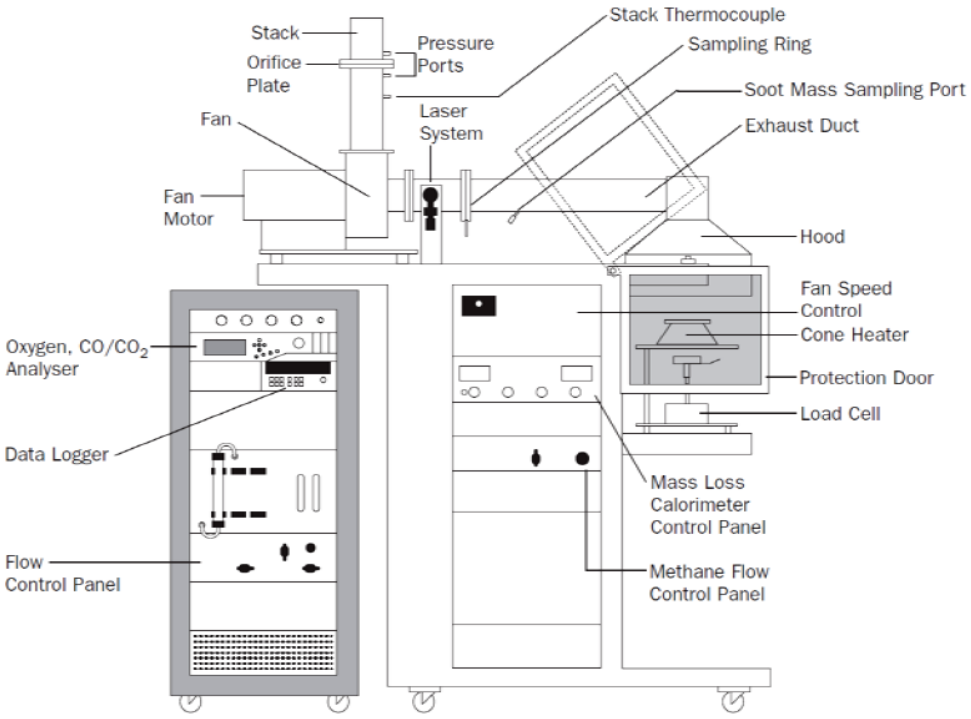

Figure 3. Illustration of the cone calorimeter and its parts, originally from Fire Testing Techonology (n.d.), modified by Lindholm et al. (2009).

The standard size of a test specimen for the cone calorimeter is 100 x 100 mm with a maximum thickness of 50 mm. The sample is placed inside a sample holder which connects to the load cell. The load cell keeps track of the weight of the sample during the burning period (Lindholm et al., 2009). The cone heater, placed horizontally above the sample, is heated to the temperature that will yield the desired heat flux at the sample surface. The intensity of heat flux provided by the cone heater ranges from 0 - 100 kWm^{-2} (Schartel & Hull, 2007). Below the cone heater is a spark igniter which will ignite the flammable gases that leaves the sample. The combustible products will travel into the hood above the cone heater and further in through the exhaust duct for analysis (Lindholm et al., 2009).

The oxygen analyser is the only needed analyser to execute fundamental cone calorimeter tests. There are additional analysers that measure for example carbon monoxide (CO) and carbon dioxide (CO_2), these are equipped to provide a deeper understanding of the combustion process and to minimize uncertainties (Lindholm et al., 2009).

The cone calorimeter provides no real flame spread and the burning of the sample is one-dimensional, meaning that the flame front penetrates the specimen depthwise through its thickness. Therefore, altering the thickness will affect the results significantly (Schartel & Hull, 2007).

2.3.1 Relation between HRR and oxygen consumption

HRR can be measured in many ways, but the most used method is oxygen consumption calorimetry (method used by the cone calorimeter). This method is based on the fact that most solids, liquids and gases have the same energy release per unit mass of consumed oxygen, see Figure 4. This value is 13.1 MJ per kilogram consumed oxygen with an accuracy of ±5 % for most fuels. The cone calorimeter measures the composition and flow rate of the combustible gases which in turn provides information on how much oxygen is consumed during combustion (Karlsson & Quintiere, 2000).

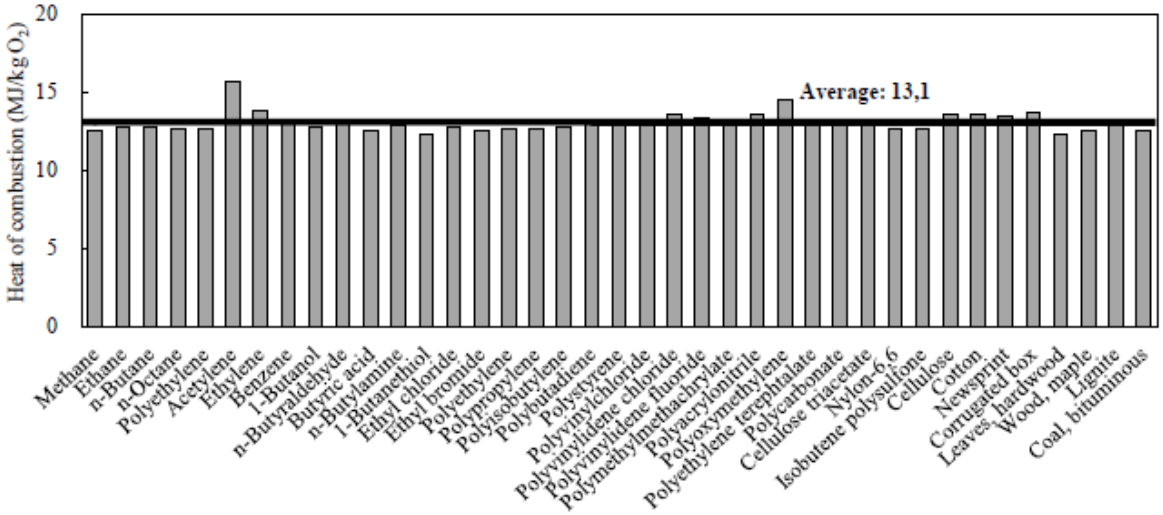

Figure 4. Calculated energy release per unit mass of oxygen consumed for different fuels. An average value for all fuels is 13.1 MJkg$_{O2}^{-1}$. Data originally from Hugget (1980), reproduced by Lindholm et al. (2009).

As the cone calorimeter cannot measure HRR directly it is calculated by Equation 2.

$$\dot{Q} = (13.1 \cdot 10^3) \cdot \Delta\eta_{O_2} \cdot \dot{V} \cdot \rho_{O_2} \quad (2)$$

where $\dot{Q}$ is HRR [kW], 13.1 MJkg$_{O2}^{-1}$ is the heat of combustion, $\Delta\eta_{O_2}$ is the measured reduction in mole fraction of oxygen in the exhaust air, $\dot{V}$ is the volumetric flow rate [m^{3}s^{-1}] and ρ_{O_2} is the density of oxygen [kgm^{-3}] (FireSUN, 2021; Karlsson & Quintiere, 2000).

2.4 Scanning Electron Microscope

In scientific evaluation it is often important to observe the microstructure and form of the analysed material. Hence, it is common to use an optical microscope or a magnifying glass. However, when using light, it is difficult to observe the nano/sub-microstructure of a material since the wavelength of light is not small enough (JEOL, n.d.). The Scanning Electron Microscope (SEM) is an instrument that uses a focused beam of electrons to scan the surface of a sample, the beam has shorter wavelength than light and the electrons possess energies up to 40 keV (Bogner et al., 2007), which makes it possible to analyse a material down to several nanometres (JEOL, n.d.). Multiple signals are produced that give information about texture, crystalline structure and chemical structure of the sample which in turn are used to generate an image (Bogner et al., 2007; Swapp, n.d.), see Figure 5. The SEM has become a necessity when it comes to studying morphology, topography, crystallography, and composition of materials. Hence, the SEM has become a popular instrument for advanced research in for example chemistry, physics, and geology (Jang et al., 2020).

When the electron beam hits the specimen multiple signals are emitted. These signals are typically backscattered electrons, secondary electrons, cathodoluminescence and characteristic X-rays which depends on the structure and density of the material as well as the different elements inside the specimen (JEOL, n.d.), see Figure 6.

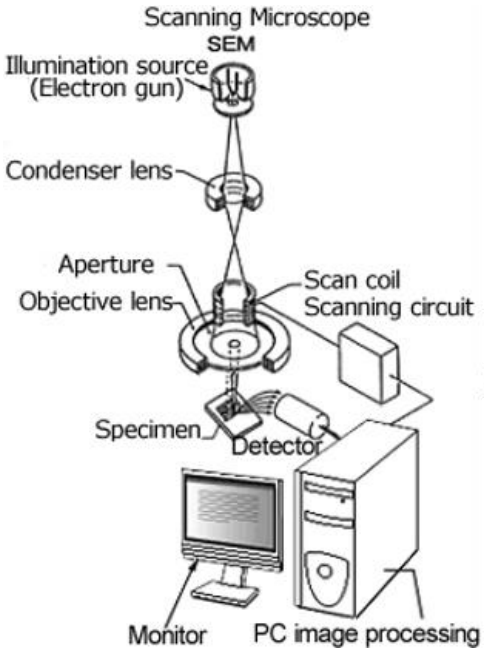

Figure 5. Ilustration of SEM, the detected signals are transferd to a computer to create an image. Originally from JEOL (n.d.).

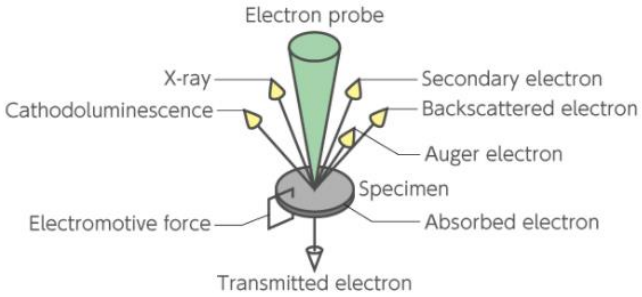

Figure 6. The produced signals from the specimen. Originally from JEOL (n.d.).

The generated images are usually formed by the detected secondary electrons or backscattered electrons where the former gives information regarding the surface and the latter information regarding the composition of the analysed sample (L-Tube, 2021). The electrons intensity varies due to the angle of the beam onto the surface of the material, this provides differences in roughness which can be observed in the images (JEOL, n.d.). The quality of the received images is dependent on multiple parameters such as brightness, working distance, contrast, and magnification (Jang et al., 2020).

2.5 Thermocouples

Thermocouples (T/C) is a useful and common instrument for measuring temperature which consist of two wires of different alloys or metals welded together. There are multiple different types of T/Cs, but type K is the most used in fire testing. It is popular since it retains its mechanical properties as well as resists corrosion at high temperatures, the melting point is at 1400 °C. However, oxidation can occur at temperatures above 800 °C which leads to measuring errors. The T/C can also age if used in temperatures above 500 °C therefore they need to be recalibrated after 20 hours of use (Wickström, 2016).

T/C with a small cross section diameter is often used since they register temperatures close to the gas temperature. A large cross section diameter adjusts closer to the temperature generated by radiation. Thus, T/Cs are affected by both incident radiation and gas temperature (Wickström, 2016).

2.6 Humidity sensor

In the laboratory work of this thesis a *Tinytag Plus 2 (TGP-4505)* was used, it is a waterproof data logger with a relative humidity (RH) and temperature probe attached to a 1.5 m cable, see Figure 7. The instrument measures temperatures between -25 to +85 °C and relative humidity from 0 to 100 %. The operational temperature limit is 85 °C which is the physical limit to which the sensor can be exposed (Gemini Data Loggers, n.d.).

Figure 7. Tinytag Plus 2 (TGP-4505) with external temperature and RH probe.

Relative humidity is a measure of the current amount of water vapour in the air expressed as a percentage of the required content to achieve saturation at the present temperature. Relative humidity is strongly related to temperature, which makes it sensitive to temperature changes, thus a stable temperature will produce a stable relative humidity (Vaisala, n.d.).

2.7 Laboratory tests

The following section present the preparation of laboratory tests and the procedure to collect data from the cone calorimeter and SEM analysis.

2.7.1 Preparation of cone calorimeter tests

Untreated spruce wood (soft-wood) with moisture content 11.2-20.8 % (Swedish Wood, n.d.) was cut into pieces of 100x100 mm with thicknesses of 10, 20 and 30 mm. The bottom of the pieces was wrapped in aluminium foil and placed on three types of material; kaowool (insulation), 8 and 20 mm pieces of steel and aluminium foil wrapped around a 10 mm thick wood piece, see Figure 8a-c. This was done to identify the effect different rear materials/substrates have on HRR. Kaowool provides little heat loss downwards while steel is much more conductive, and the aluminium foil wrapped around wood provides the same thermal properties as the wood sample itself where the only difference is that no further combustion will take place.

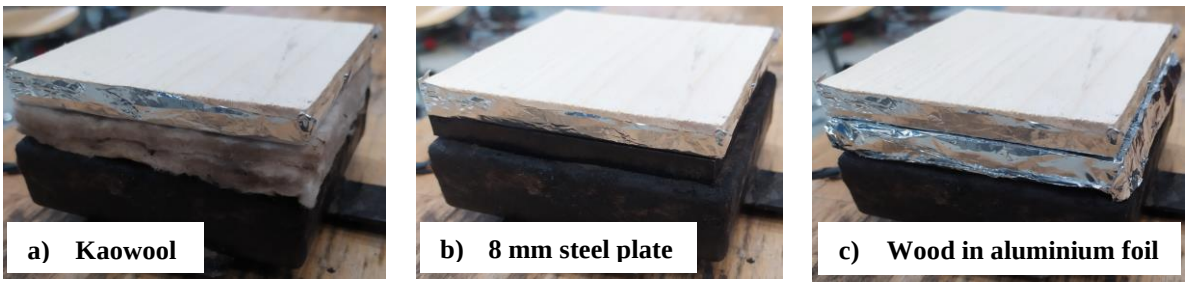

Figure 8. Sample setup. a) two layers of Kaowool on the rear side of the sample, b) 8 mm steel plate on the rear side of the sample and c) aluminium foil wrapped around a 10 mm thick piece of wood on the rear side of the sample.

Table 1 shows the setup of rear material and dimensions that was used for the three thicknesses of wood. The standard number or replications is three when using the cone calorimeter, therefore each test was replicated at least three times, see Table 2.

Table 1. Setup of rear materials in samples.

Material and piece dimensions	**Wood sample**		
	10 mm	20 mm	30 mm
Kaowool (1 piece: 100x100x8 mm)	2 pieces	2 pieces	2 pieces
Steel plate (1 piece: 100x100x8 mm)	1 piece	-	1 piece
Steel plate (1 piece: 100x100x20 mm)	1 piece	-	-
Aluminium foil around wood (1 piece: 100x100x10 mm)	1 piece	-	1 piece

Measurements of HRR, temperature and humidity as well as SEM analysis were performed on the samples according to Table 2. Measurements of HRR and temperature were also performed on samples of low moisture content and the results are presented in section 4.1.5. The progression of the char zone during certain stages of the second PHRR was analysed, and the results are found in section 4.2. To prepare the samples for the SEM analysis, liquid nitrogen was poured on top of the samples to immediately stop the burning process, this is explained further in section 2.7.2 and the results are found in section 4.4.

Table 2. Dimensions and number of spruce samples per test in the cone calorimeter. Three types of rear materials were used, namely kaowool, 8 and 20 mm steel plates and aluminium foil wrapped around a piece of wood. Measurements were also performed on samples of low moisture content (dry), samples that were used to analyse the char progression during the second PHRR and samples where the flames were put out with liquid nitrogen.

	Number of wood samples (100x100x*thickness below* mm)						
	10 mm	20 mm	30 mm	HRR measurement	Temperature measurement	Humidity measurement	SEM analysis
Kaowool	3	3	3	✓	✓	✓	
8 mm steel plate	3	0	3	✓	✓		
20 mm steel plate	3	0	0	✓	✓		
Aluminium foil around wood	3	0	3	✓	✓		
Kaowool – Dry sample	3	3	3	✓	✓		
Kaowool – Progression of char zone	3	3	0	✓			
Kaowool – Liquid nitrogen	6	0	0	✓			✓

HRR and temperature

The wood samples were weighed and measured before they, together with the rear material, was placed on the base of the sample holder. A thermocouple of type K with wire diameter 0.25 mm was then inserted between the sample and aluminium foil, see Figure 9a, this was done to create a temperature profile of the fire scenario. The last step was to place the lid of the sample holder onto the sample, see Figure 9b.

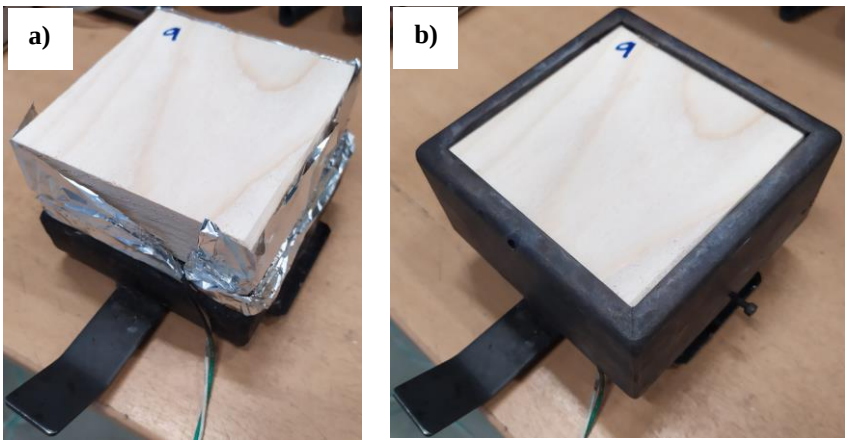

Figure 9. a) Sample wrapped in aluminium foil and placed on the base of the sample holder. A thermocouple is inserted between the aluminium foil and wood sample. b) Sample ready for analysis. The lid of the sample holder is placed on the sample.

Figure 10 provides a detailed description of the samples, below the figure is an explanation of each part.

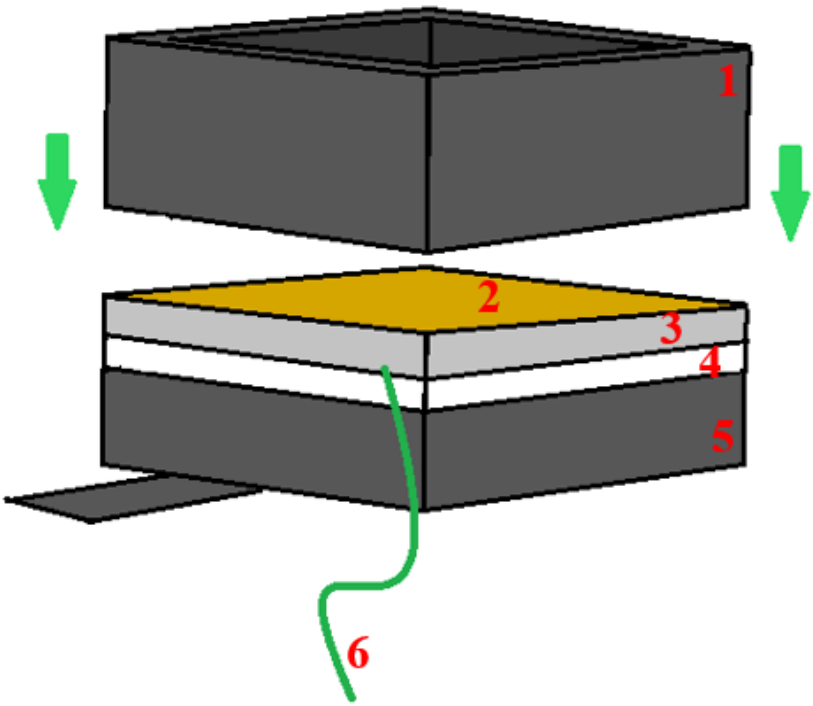

Figure 10. Set up of samples. See below for an explanation of each part.

1. Lid of the sample holder that slide on top of the sample exposing the sample surface.
2. Wood sample, 100x100 mm with thicknesses of 10, 20 and 30 mm.
3. Aluminium foil wrapped around the wood sample.

4. Kaowool, steel plate or aluminium foil wrapped around wood depending on the analysed sample (see Table 1 for dimensions).
5. Bottom part of the sample holder with a handle to easily move the sample in and out of the cone calorimeter.
6. T/C, type K with wire diameter of 0.25 mm.

The helical coil of the calorimeter was set to 722 °C which corresponds to a heat flux of 35 kWm^{-2} and the exhaust duct flow rate was 24 ls^{-1}. The computer connected to the cone calorimeter was adjusted to calculate HRR each 5 s, this was calculated from the data collected through the consumption of oxygen. The computer program *Easyview* was used to measure the temperature during the test. The program was set to collect new values each second providing a temperature curve of the fire scenario. Thus, HRR was calculated each 5 s and temperature measured each 1 s.

Before the tests could begin the sample holder (without the wood sample) needed to be placed on the scale under the cone in the cone calorimeter, the weight was then tared so the instrument could measure the mass loss rate of the sample during the test. When this was done the actual sample was placed in the cone calorimeter horizontally, see Figure 11a. Thereafter, the covers with ceramic insulation, placed directly under the cone, were pushed to the sides exposing the sample surface to radiation from the cone and the spark igniter was placed above the centre of the specimen, see Figure 11b. At the same time the collection of data was initiated. As soon as the sample ignited the spark igniter was removed and the time for ignition was noted. The wood was left to burn until flameout occurred.

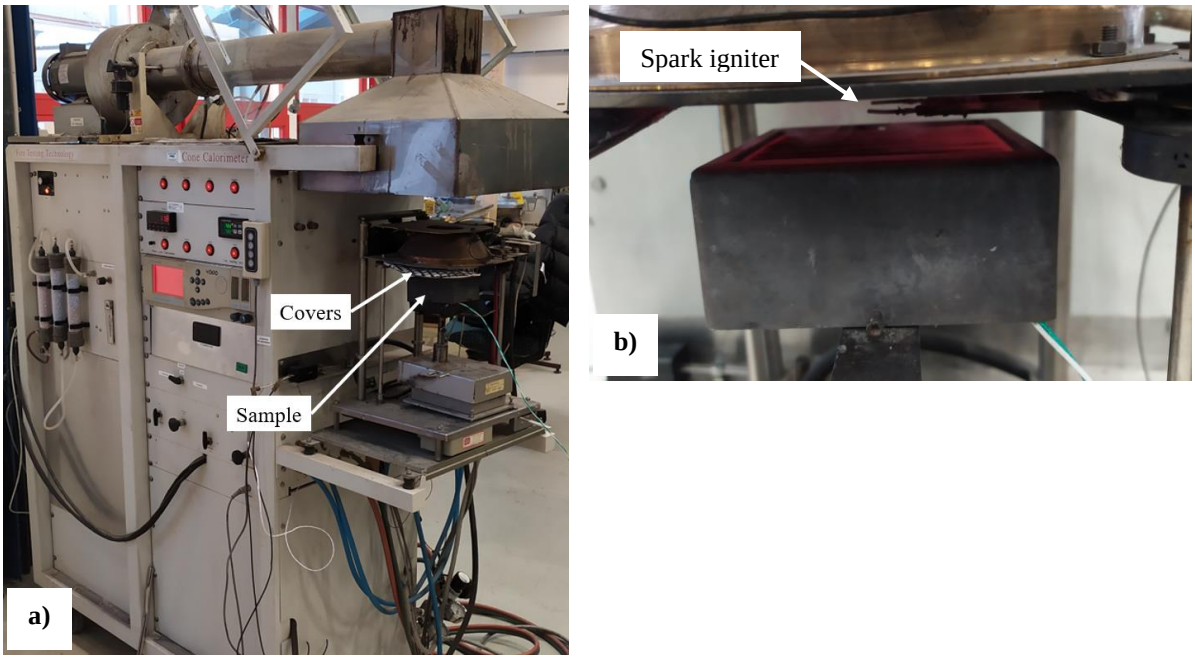

Figure 11. a) Sample placed on the scale in the cone calorimeter. b) Sample exposed to radiation with the spark igniter placed above the centre of the specimen.

10, 20 and 30 mm thick samples were also dried in an oven at 100 °C for over one week. These samples where then tested with the same procedure as previous tests to calculate and measure HRR and temperature.

The progression of the char zone during the second PHRR was observed by ending the cone calorimeter tests prior to, during and after the second PHRR. Water was poured on the sample surface to stop the burning process, thereafter the sample was quickly sawed apart to observe how far the char zone had reached.

Moisture transport

The used humidity sensor was *Tinytag Plus 2 (TGP-4505)*, which is a waterproof data logger with a relative humidity and temperature probe. To avoid damaging the cable through heat radiation, insulating kaowool (8 mm) was wrapped around the base of the cable leaving the sensor exposed. The wood sample was then placed in the lid of the sample holder and the probe was inserted to the centre of the sample backside through a hole in the side of the lid, see Figure 12a. Thereafter, the lid was placed on top of the two pieces of kaowool and base of the sample holder, see Figure 12b.

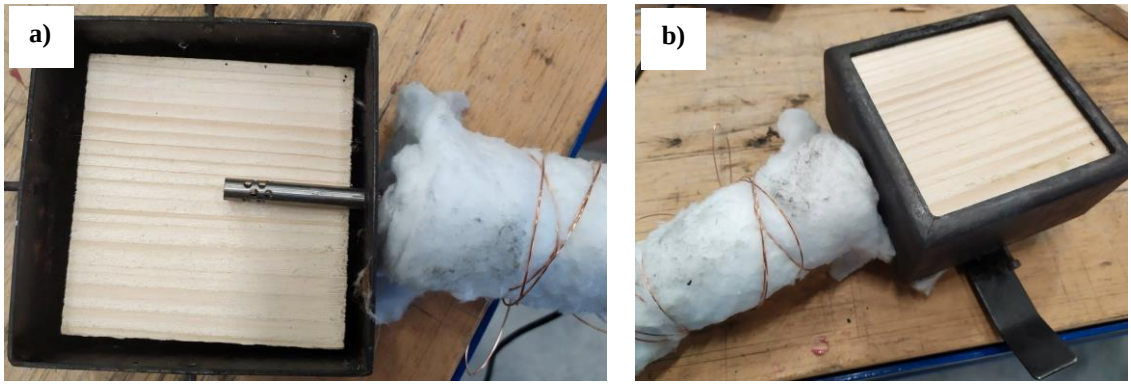

Figure 12. a) Humidity sensor placed at the centre of the rear side of the wood sample. b) Sample ready to be placed in the cone calorimeter.

The cone calorimeter settings used in the HRR and temperature tests were kept the same. The computer program *Easyview* was used to measure the relative humidity/moisture transport during the test and new data was collected each second. Measurements could only be recorded until the temperature of the sensor reached 60 °C since the humidity sensor has an operational range of -25 to +85 °C. Cancelling the test when the sensor reached 60 °C provided time to disassemble the sample holder and remove the probe without damaging it.

The sample was mounted, and tests were started with the same procedure as the HRR and temperature tests mentioned above. Wood pieces was placed under the cable for support and to keep the kaowool in place, see Figure 13.

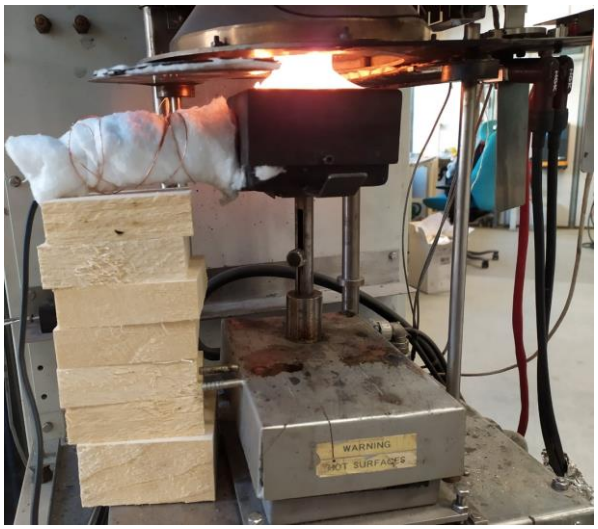

Figure 13. Sample placed in the cone calorimeter. The humidity probe is seen to the left where it is inserted through the side of the sample holder.

2.7.2 Preparation of Scanning Electron Microscope tests

Samples were prepared for SEM analysis by removing the wood sample before and after the second peak on the HRR curve, three samples each were removed before and after the peak. Liquid nitrogen was poured on the top of the samples to stop the burning process at the sought-after stage. Water was not used as it would damage the surface of the char. The liquid nitrogen evaporated immediately inflicting less damage to the char structure.

The SEM model was JEOL JCM-6000 Tabletop SEM, Figure 14a. The samples for the SEM were prepared by first placing a carbon stub (double adhesive tape that is conductive) on the sample holder, see Figure 14b. Thereafter, bits/fragments of char and fresh wood were taken from the samples and mounted on to the carbon stub and placed inside the chamber of the SEM, see Figure 14c. The samples were placed top down to receive an image of the surface of the specimen.

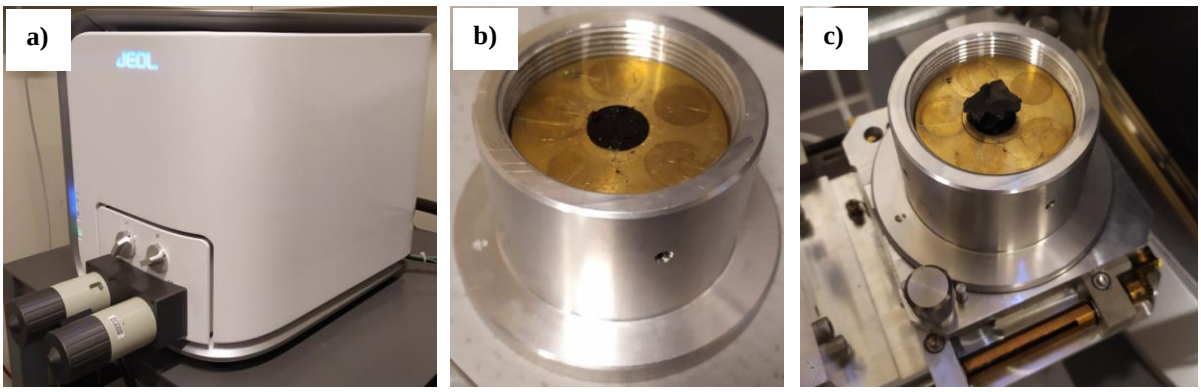

Figure 14. a) JEOL JCM-6000 Tabletop SEM. b) Carbon stub placed in the centre of the sample holder. c) Char sample mounted on the sample holder and placed in the chamber of the SEM.

The SEM settings were set to low-vacuum, acceleration voltage to 15 kV, high probe current and standard filament current. The images were generated from the detected signals of backscattered electrons.

3 Theoretical framework

The following section presents the theoretical framework of the study. Providing a deeper understanding of wood and its decomposition process as well as HRR.

3.1 Wood

According to Svenskt trä (2020) wood has become an increasingly important topic when it comes to building a sustainable society with a responsible use of the earth's resources. Wood has the environmental benefit of being renewable and formed naturally in an ecological cycle that absorbs carbon dioxide (CO_2). In addition, wood is a strong building material in relation to its weight, which is well suited for construction (Svenskt trä, 2020).

3.1.1 Fire properties

The surface of wood can ignite when exposed to fire. The specific fire properties of wood depend on the type of wood species and its dimensions. Thin wood ignites easily while wood with thicker dimensions is harder to ignite and burns with a slow rate (Svenskt trä, 2016). Moreover, ignition depends on multiple factors including moisture content, grain orientation, exposure conditions, density and the wood's inherent variability as a natural material (Spearpoint & Quintiere, 2001).

Svenskt trä (2016) and Lowden and Hull (2013) describe the thermal decomposition process of wood with different temperature zones. A rephrased summary of this is presented in Table 3.

Table 3. The decomposition process of burning wood. Rephrased from Svenskt trä (2016) and Lowden and Hull (2013).

Temperature range	**Decomposition process**
>100 °C	Chemically unbound water evaporates
160-200 °C	The decomposition is slow and mainly non-combustible gases, such as water vapour and CO_2, are produced.
200-225 °C	Slow wood pyrolysis. Gases produced are still non-combustible.
225-275 °C	Main pyrolysis starts. Flaming combustion occurs.
280-500 °C	A greater number of combustible gases are emitted which will ignite and burn at the outer edges of the material if oxygen is provided. A layer of char will quickly begin to form as the materials physical structure breaks down. Smoke particles will be visible, and the produced gases will now be volatile (for instance methane and CO).
>500 °C	The char layer will start to smoulder, and the combustion process will proceed in the same rate as the layer forms. The production of volatile substances is complete and the char will oxidise to form H_2O, CO_2 and CO until nothing but ashes remain.

When ignited, the combustion process will proceed inwards at a constant rate. However, the penetration is slow since the char layer acts as insulation, which counteracts the heat flow from the fire into the wood pyrolysis zone, see Figure 15 (Svenskt trä, 2017).

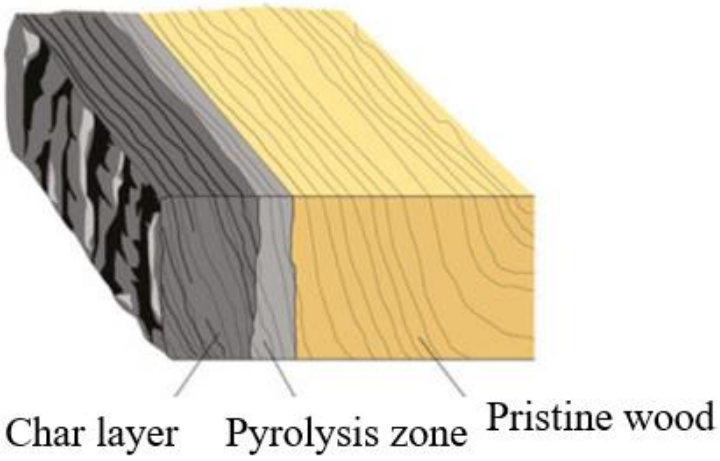

Figure 15. The char layer protects the inner wood which maintains its stability and load-bearing capacity. Originally from Svenskt trä (2019), translated into English.

3.1.2 Char

Charring is a process that begins on the wooden surface when it is exposed to fire or high temperatures. When ignited the burning of the pyrolysis zone starts, which results in the release of heat. Soon after ignition the charring process initiates and the heat released from the material is reduced, indicating that the char layer has protective and insulating properties, see Figure 16 (Svenskt trä, 2016).

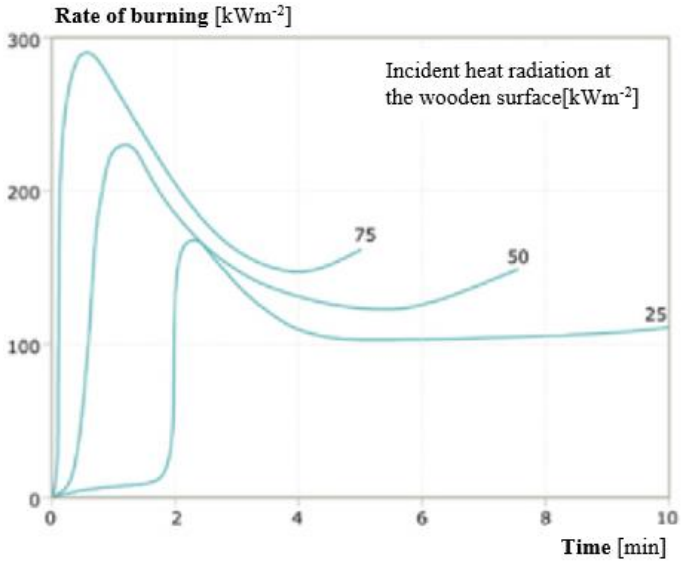

Figure 16. Rate of burning from a wooden surface. Originally from Svenskt trä (2016), translated into English.

During fully developed fires the rate of charring is normally ca. 0.6-1.0 mm/min (Svenskt trä, 2016). However, this rate can vary depending on factors, such as density, oxygen concentration, moisture content, thickness of the char layer and external heat flux (Lowden & Hull, 2013). Beneath the layer of char is the pyrolysis zone with a thickness of only a few millimetres. The wood in this region is affected by the high temperatures, which in turn deforms the material at a constant rate. Below this zone is virgin wood at normal temperatures, meaning that the properties of the material in this area have not changed. Hence, wooden constructions, with sufficient thickness, retain their load-bearing capacity for a relatively long period of time (Svenskt trä, 2016). However, the layer of char does not strengthen the material but will only act as thermal resistance between the pyrolysis zone and the underlying wood. Hence, it contributes to a decrease in HRR and will work as a barrier for mass transport of combustible gases released from the material and oxygen from the air (Lowden & Hull, 2013). Once a layer of char has formed there are significant differences in the heat transfer mechanism that heat the virgin wood. Heating of virgin wood is

mainly done by conduction but in the case of char it is radiative heat transfer through the pores that is dominating (Bartlett et al., 2019).

According to Lowden and Hull (2013) the production of char is dependent on the time and rate of heating. Char formation is also due to the polycondensation reactions of mainly lignin, which can occur at high temperatures (>500 °C). Furthermore, the char structure varies widely with wood species, heating rate, fire retardant treatment, density, oxidation resistance, permeability, thermal insulation properties, etc.

3.1.3 Pyrolysis

Changes in the wood structure occurs when wood is exposed to high temperatures. There are three biopolymeric components in wood, namely lignin, cellulose, and hemicellulose. As the temperature rises these components decompose into combustible gases, carbonaceous char and tar. It is this process that is called pyrolysis and takes place beneath the layer of char (Lowden & Hull, 2013). The pyrolysis zone is only a few millimetres thick and according to Lowden and Hull (2013) the temperature of the zone is much lower than the temperature of the char layer, hence, whilst the char can reach temperatures of 800 °C the pyrolysis zone will only reach temperatures of approximately 225-500 °C.

If the heating rate is quick pyrolysis can occur before the material has dehydrated, however, the process will be faster if the material is dry i.e. has low moisture content (Bartlett et al., 2019). Wood undergoes different stages of pyrolysis explained in Table 3.

3.1.4 Effects of thermal degradation

Försth and Roos (2011) introduce an interesting finding in their article which is absorptivity and its dependence on heat source. According to the authors, different surfaces will absorb a non-equal amount of heat when exposed to radiation. The surface will heat up and ignite depending on the absorptivity. It is commonly known that a dark surface absorbs more heat from visible light than bright surfaces. However, when considering radiation from fires the spectral blackbody exitance has its maximum at 2µm, this lies in the infrared (IR) part of the spectrum, meaning that the colour of the surface is less relevant. Försth and Roos (2011) studied plywood and found that with longer exposure time the absorptivity in the IR spectrum decreases while it increases in the visible spectrum, see Figure 17. This indicates that the layer of char will decrease both the absorptivity (Försth & Roos, 2011) and HRR as less heat is absorbed and therefore less heat can be released.

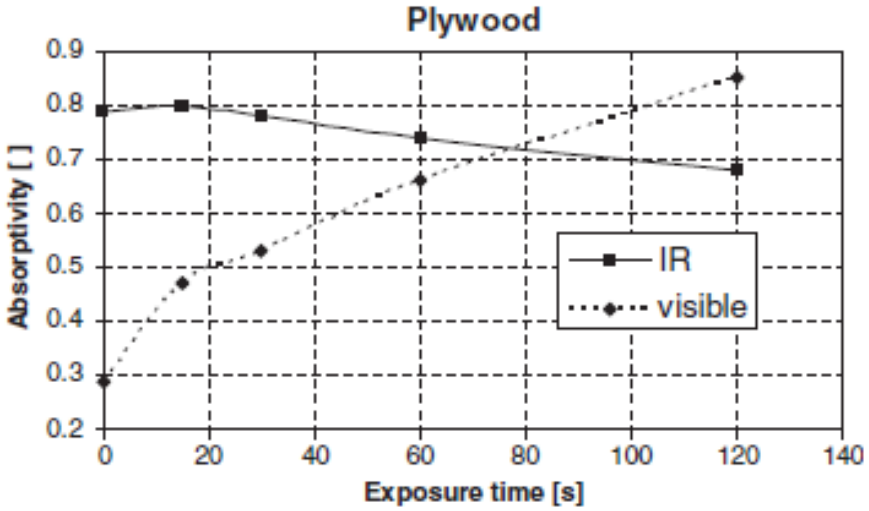

Figure 17. Effective absorptivity over time originally from Försth and Roos (2011), reproduced with permission. The data was collected from a plywood sample exposed to a heat flux of 30 kWm^{-2} in a cone calorimeter.

3.1.5 Moisture properties and transport

Wood is a hygroscopic material meaning that it absorbs moisture from the surroundings. The exchange of moisture between air and wood is dependent on the relative humidity in the air, current moisture content in the material and temperature (Forest Products Laboratory, 2013). According to Forest Products Laboratory (2013) the amount of water in wood can induce challenges in construction as the water influences the properties of the material.

Wood contains many pits (holes) and lumina (tubular channels), see Figure 18. Lumina have diameters of 10-70 µm creating a porous structure, which provides the material with oxygen (Gan et al., 2019). As wood is a hygroscopic material there are different ways for water to enter the material: water can go through the cell lumens as fluid by capillary action or as vapour, but also through molecular diffusion in the cell walls (Puuinfo Ltd., 2020).

Wood expands and contracts in different directions of the growth rings and the grain when moisture is added or removed, see Figure 19. The materials ability to release and absorb water is beneficial in construction as the moisture content prolongs ignition time while dry wood has a significantly improved strength in compression and bending (Puuinfo Ltd., 2020).

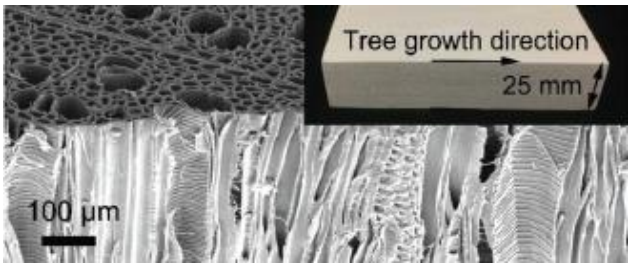

Figure 18. Microscopic structure of wood showing the lumina. Originally from Gan et al. (2019), reproduced with permission.

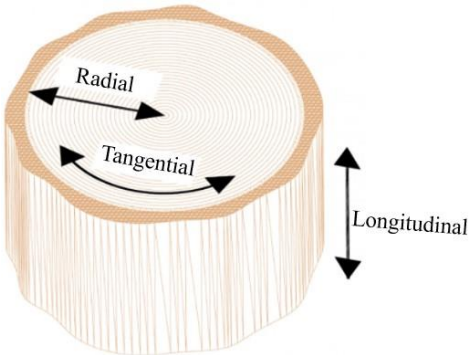

Figure 19. Wood expands and contracts in different directions when moisture is added and removed from the material. Modified but originally from Puuinfo Ltd. (2020).

Upon heating, water begins to evaporate from the wood when the temperature within the material approaches 100 °C. Some water vapour will leave through the surface of the material whilst some will migrate away from the heat source and deeper into the material where it re-condenses. This produces three zones as illustrated in Figure 20: A dry zone where the pyrolysis takes place, a dehydration zone, and a wet zone (Bartlett et al., 2019).

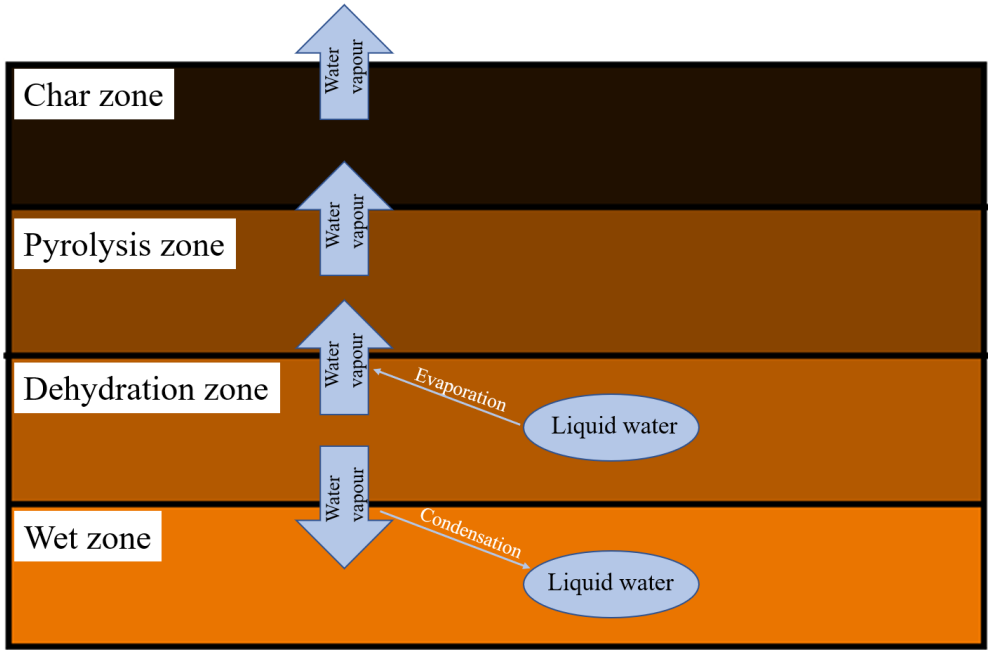

Figure 20. Moisture transport within a burning wooden sample.

Pyrolysis and dehydration can occur simultaneously if the heat flux is high enough. At this stage the moisture will slow the temperature rise in the material since the supplied energy will be used to evaporate the water instead of heating the specimen. Thus, greater moisture content increases the energy needed to evaporate the water, hence, less energy is accessible for pyrolysis. Furthermore, the mass flow of water vapour through the material will also cool the pyrolysis zone and slow down the charring rate (Bartlett et al., 2019).

A high moisture content prolongs the time to ignition and slows speed of pyrolysis. Therefore, wood with 12 % moisture content will ignite after almost double the time as that of dry wood (Bartlett et al., 2019).

3.2 Heat release rate

HRR indicates the amount of released energy per unit time for a given burning object. According to Fateh et al. (2014) energy released in a compartment fire gives information on fire properties such as hot gas temperatures, plume flows and rate of descent of hot gas layers. Fire development is often characterized in terms of HRR versus time, thus HRR is one of the most valuable variables when it comes to evaluating material fire hazards (Fateh et al., 2014). If a material has a quick release of its potential chemical energy as well as toxic gases and smoke it is considered more hazardous than materials which has a slower release. According to Forest Products Laboratory (2013), HRR describes the general combustion behaviour whilst the peak heat release rate (PHRR) is the maximum HRR, an important parameter that is used to evaluate the flammability of a material. Time to ignition (TTI) and time to PHRR (TPHRR) describes the time it takes to reach ignition and PHRR, respectively (Das et al., 2017).

3.2.1 Heat release rate of Wood

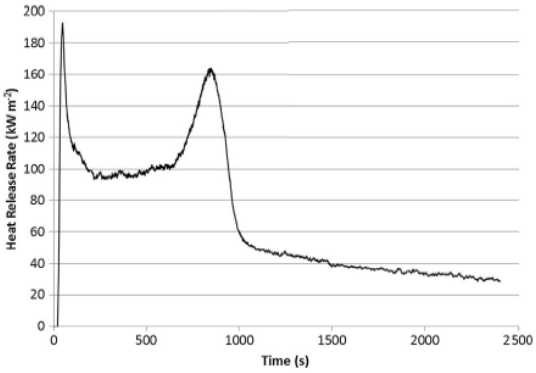

Figure 21. Heat release rate of scots pine sapwood subjected to heat flux of 50 kWm^{-2} in a cone calorimeter (Lowden & Hull, 2013).

Wood is a material with thick charring and over time its HRR curve tends to peak at the start where no charring has yet occurred as well as at the end of the combustion, an example of this is visualised in Figure 21 (Lowden & Hull, 2013).

According to Lowden and Hull (2013) the first peak is a response from ignition of the surface. The generated heat from combustion will maintain the pyrolysis of the material and release more volatile gases. The decrease in HRR is caused by the formation of char layer that has an insulating effect slowing down the pyrolysis process as well as hindering the transport of heat and pyrolysis gases through the material. The second peak is believed to be a result of material burn through and char cracking, which enable the escape of additional volatile gases. The final decrease in HRR occurs when no more volatiles are released and the flaming combustion ends, resulting in a steady baseline.

Sample burn through

Similar to Lowden and Hull (2013), Tran (1992) suggests that the second peak is a result of a raise in bulk temperature of the remaining material when the pyrolysis zone reaches the rear side of the sample. Tran argues that if the material is sufficiently thick, the second peak will not occur. Tran tested two thicknesses of red oak wood, namely 18 mm and 64 mm. The sample which was 18 mm (analysed with a cone calorimeter) showed a second peak while the sample having 64 mm thickness (analysed with the Ohio State University (OSU) heat release rate apparatus), that was only analysed until the char depth reached 36 mm, didn't experience a second peak.

Forest Products Laboratory (2013) agrees that burn through is the reason for the second HRR peak. Forest Products Laboratory (2013) suggests that the peak is an effect of the pyrolysis zone reaching the sample's rear side, which increases both temperature and HRR. Forest Products Laboratory (2013) studied HRR when a sample is exposed to different heat flux intensities. Results shown in Figure 22 indicate that a higher heat flux give quicker and higher HRR peaks,

meaning that burn through and flameout takes place earlier when exposed to high temperatures and heat flux.

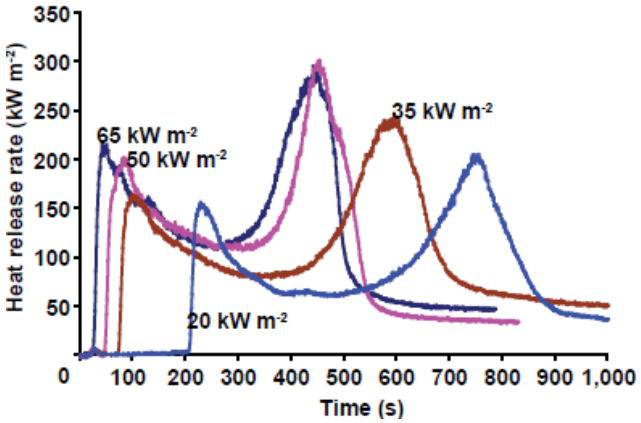

Figure 22. HRR as a function of time. A sample is exposed to different heat fluxes ranging from 20-65 kWm-2 originally from Forest Products Laboratory (2013).

Char

Gan et al. (2019) studied HRR difference between normal wood and densified wood. The densification of wood was created through a process of mechanical pressing, which removed the porous structure of the normal wood, leaving no channels in the structure, see Figure 23a-b.

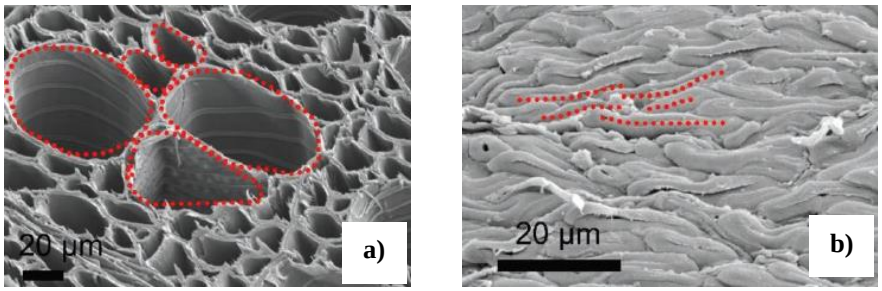

Figure 23.a) Microscopic structure of normal wood, red dots outline holes in the char structure. b) Microscopic structure of densified wood, red dots outline collapsed wood channels of the char structure. Originally from Gan et al. (2019), reproduced with permission.

When analysed it was proven that PHRR occurred much later and at a lower value in the case of densified wood compared to normal wood, see Figure 24. The second HRR peak is, according to Gan et al. (2019) , caused by cracks forming in the char layer, creating an easy pathway for the combustible gases inside the wood, and as the cracks grow larger the PHRR is reached. The char layer of the densified wood is very strong, this results in a reduction in the flow rate of combustible gases, which maintains the HRR at a low level. As the cracks form in the char layer, they will not grow as deep and wide as in normal wood due to the dense structure of the material, therefore the PHRR is not as large as that of normal wood. The porous structure of normal wood is more flammable as it contributes with a greater presence of oxygen, which increases burning and consequently HRR.

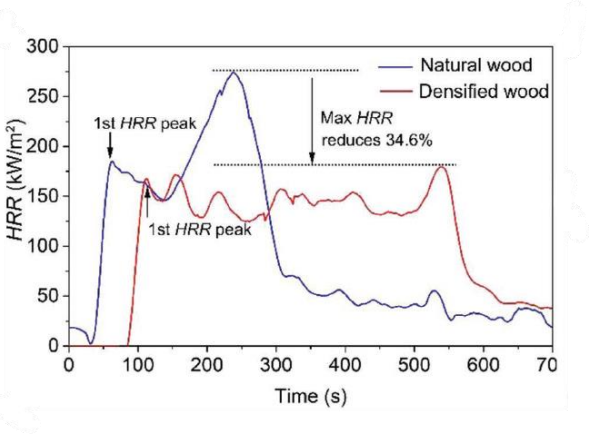

Figure 24. HRR as a function of time for normal and densified wood, originally from Gan et al. (2019), reproduced with permission.

However, Bartlett et al. (2019) also studied the effect of density on charring rate and mass loss rate. Herein, it was discovered that higher density decreases charring rate, seen in Figure 25a. Bartlett et al. (2019) argue that higher density generates char at a slower pace as more energy is required to pyrolyze a greater material mass. However, MLR increases with denser materials as shown in Figure 25b. This indicates that overall pyrolysis increases, which results in a greater contribution of combustible gases.

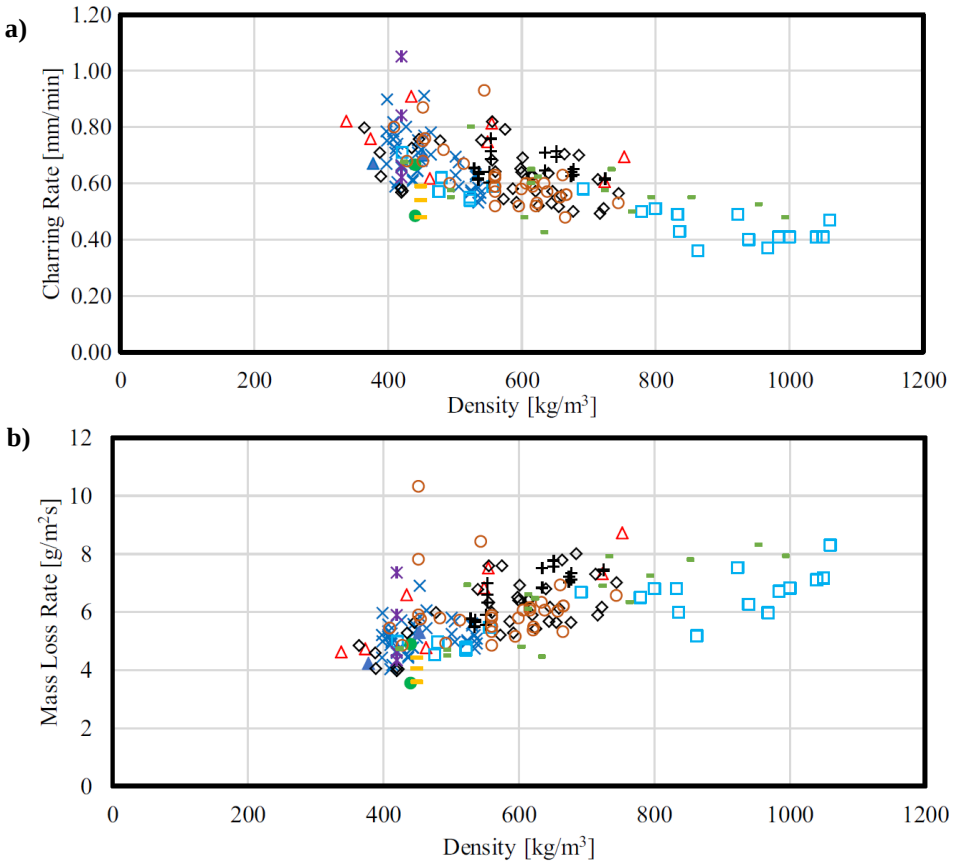

Figure 25. a) Charring rate as a function of density. b) MLR as a function of density. Originally from Bartlett et al. (2019).

This is interesting since MLR is closely related to HRR, see Equation 1, meaning that higher density leads to higher HRR, which in that case is contrary to what was mentioned by (Gan et al., 2019), who suggested a lower HRR with higher density.

3.2.2 Comparison between HRR of wood and charring/non charring thermally thick materials

Schartel and Hull (2007) presented HRR curves of samples of thermally thick charring and non-charring materials. The thermally thick non-charring sample, see Figure 26a, shows an end peak in HRR similar to the HRR curve of wood. The end peak is believed to be an effect of the pyrolysis zone reaching the rear side of the sample, the insulating material beneath the sample prevents downward heat transfer, which increases the HRR. Figure 26b shows the HRR curve of a thermally thick charring material where the material does not experience an end peak and as the layer of char thickens, the HRR decreases.

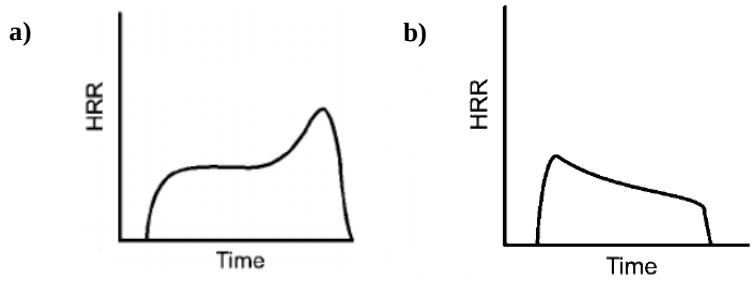

Figure 26. a) Heat release rate of thermally thick non-charring samples. b) Heat release rate of thermally thick charring samples. Originally from Schartel & Hull (2007), reproduced with permission.

This indicates that the layer of char may or may not have a great influence on the end peak of the HRR curve. The thermally thick non-charring material shows that char cracking is not needed for the sample to experience an end peak and the peak will only appear when the pyrolysis zone reaches the rear side of the sample. However, the thermally thick charring material indicates that a layer of char prevents an end peak from occurring. This is contrary to the notion that sample burn through is the reason for a second HRR peak.

3.2.3 Heat release rate of wheat gluten polymer

Das et al. (2020) gave an insight into how different char structures effect HRR. Das et al. (2020) studied wheat gluten, a bio-based polymer received as a side-stream product from food processing industries and agriculture (Kim et al., 2020), that can be used as a matrix for biocomposite. Biocomposites must satisfy the regulations of fire safety to be applied in building materials and therefore Das et al. (2020) investigated different additives in gluten polymer to improve the fire retardancy.

Figure 27 shows that the samples had many peaks in their HRR curves. Das et al. (2020) explains the initial peak as a response from ignition, subsequently char formation begins, which induce a decrease in HRR. As the cone calorimeter provided continued heat, the char layer became damaged leading to an increment in HRR. Thus, the multiple peaks are an outcome of char damage.

Figure 28 shows the char of the burnt samples as observed through SEM. The char of neat WG had multiple holes that made the char fragile and enhanced the exchange of volatiles and heat, resulting in an increased HRR. When fire retardants such as Tetra-bromobisphenol (TBBP) and Hexabromocyclododecane (HBCD) were applied, the sample char consisted of fewer holes, which led to lower HRR. The sample of wheat gluten with lanosol (WGL) had the least holes and cracks. Its char was rigid and dense and could thereby trap volatiles and resist heat damage more efficiently; hence the sample experienced the lowest HRR (Das et al., 2020).

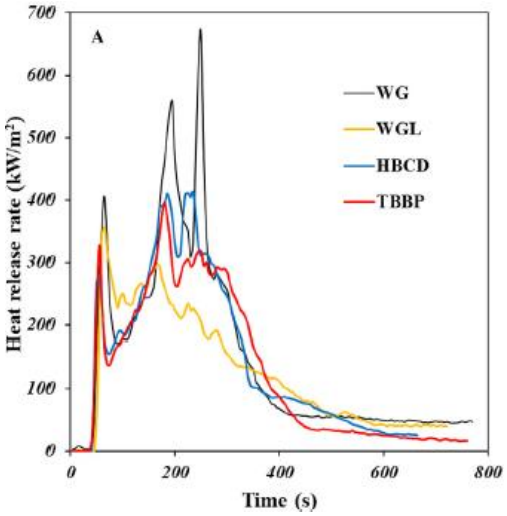

Figure 27. HRR as a function of time. WG experiences the highest HRR and WGL the lowest. Originally from Das et al. (2020), reproduced with permission.

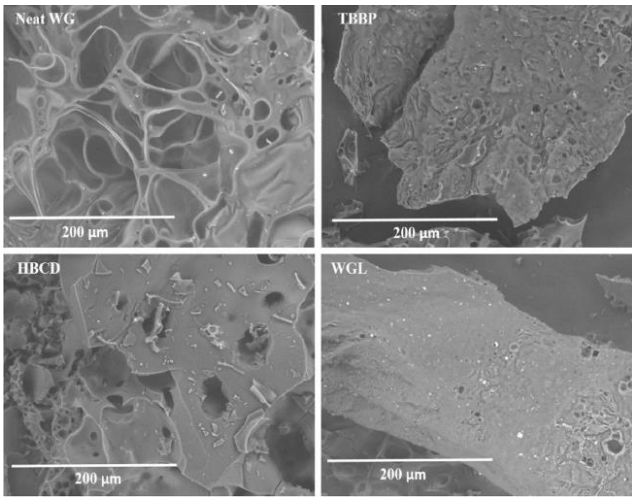

Figure 28. SEM images of the different samples and additives. WG is made up of the largest holes while WGL has the least holes. Originally from Das et al. (2020), reproduced with permission.

From literature review it is clear that researchers are equivocal about the reason for the end or second PHRR of wooden materials. This warrants a systematic study that will shed some light on the dominant mechanism responsible for the occurrence of the end PHRR peak, as commonly observed in cone calorimeter experiments.

4 Result

Heat release rate, temperature and moisture transport were measured and SEM analysis was performed for spruce wood according to section 2.7.

The samples were tested with kaowool, steel plates of 8 and 20 mm thicknesses and aluminium foil wrapped around a 100x100x10 mm wood piece on the rear side of the samples during analysis. Measurement of HRR began as soon as the sample was exposed to radiation and continued until flameout. The samples used for SEM analysis were prepared by removing three samples from the cone calorimeter before and after the second PHRR. Relative humidity/moisture transport was only measured until the temperature reached 60 °C to not risk damaging the humidity sensor.

4.1 Heat release rate and temperature vs. rear material/substrate

The following section present the result of HRR and temperature on both normal and low moisture content spruce wood.

4.1.1 Kaowool

Wood samples having thickness of 10, 20 and 30 mm were tested with kaowool on the rear side of the sample until flameout. The ignition time varied between 25-40 s, this might be due to a small difference in distance between the samples and the cone heater. When a new sample thickness is placed in the cone calorimeter the height of the load cell is adjusted, which may result in a few millimetres divergence. Other factors may also be a natural variation between the samples or, according to Spearpoint and Quintiere (2001), due to the sample warping towards or away from the cone heater resulting in a shorter or longer ignition time. Figure 29 shows the mean value (the prominent curves) and standard deviation (the shaded region surrounding the curves) of the HRR measurement. The HRR curves of 10 and 30 mm is represented by three tested samples of each thickness. However, the 20 mm HRR curve is only represented by two samples since one sample showed an unrealistic HRR curve.

The initial PHRR occurred at 35-60 s for all sample thicknesses and reached a HRR between 161-202 kWm^{-2} explicated in Figure 29. The 10 mm samples attained the highest and quickest second peak at 450 s with a HRR of 160 kWm^{-2}. The 20 mm samples experienced the second highest peak at 685 s with a HRR of 134 kWm^{-2}. Finally, the 30 mm samples had the lowest second PHRR of 78 kWm^{-2} at 1740 s.

Temperature on the rear side was recorded for all samples. However, it was observed that the temperature curves differed between the tests of each composition, it was therefore impossible to create a mean value-temperature curve. Hence, Figure 30 presents one curve from each set of tests that is closest to the mean value. All temperature curves can be seen in Appendix A – Kaowool. Figure 30 indicate that a 10 mm sample had a faster increase in temperature compared to 20 and 30 mm samples. Moreover, the temperature of all samples raised to roughly the same value of 527-560 °C at the time of flameout. Flameout occurred at the steep decrease in temperature seen in Figure 30, and at this time the samples were also removed from the cone calorimeter.

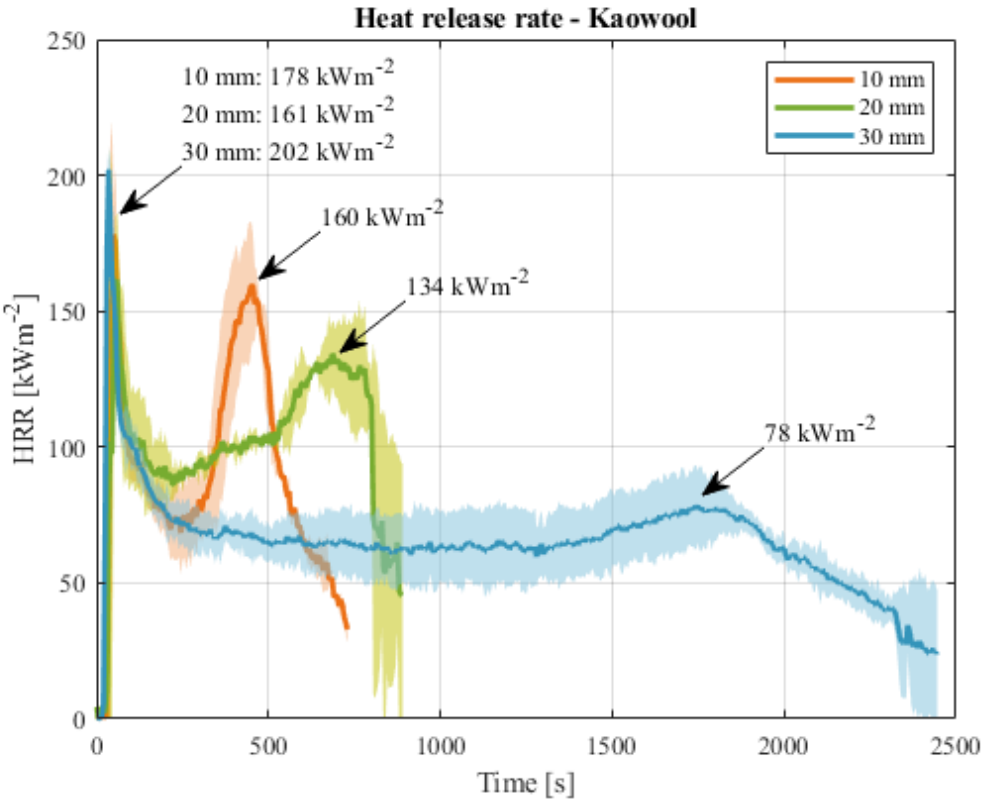

Figure 29. Mean value of HRR as a function of time for 10, 20 and 30 mm wood samples with kaowool on the rear side. Standard deviation is calculated and shown by the shaded area.

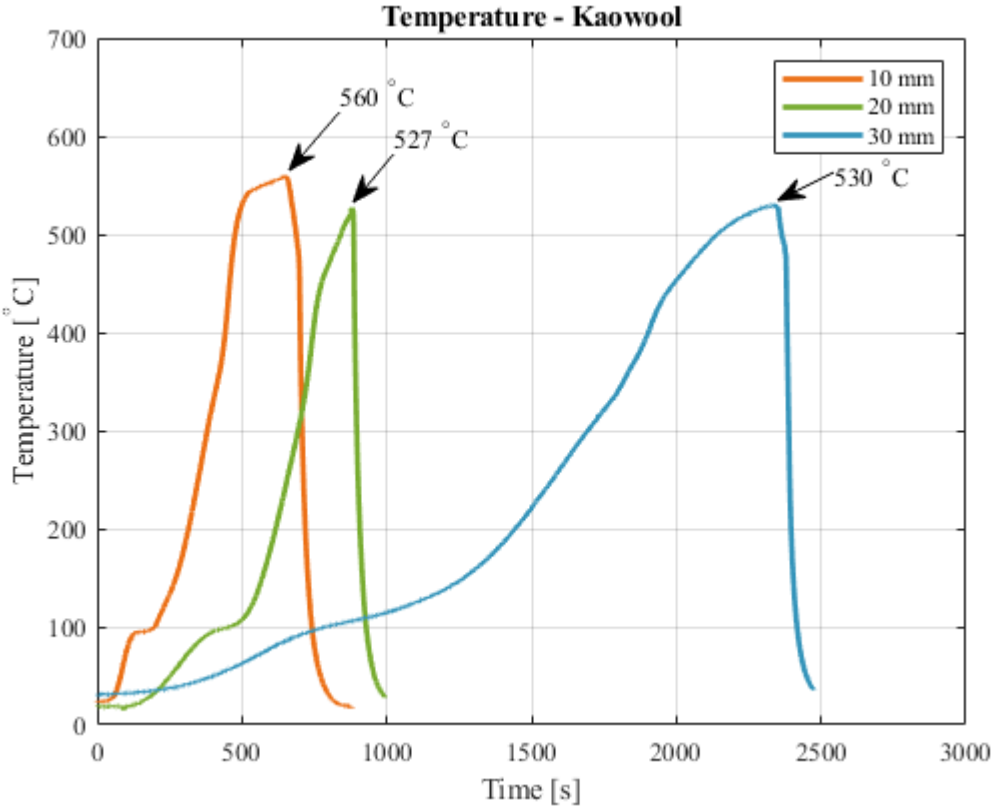

Figure 30. Temperature as a function of time for 10, 20 and 30 mm wood samples with kaowool on the rear side. Each curve represents one sample of each sample-composition.

Figure 31 shows the different stages of the HRR curve for a 10 mm sample with kaowool on the rear side. Figure 31a present the initial PHRR where the entire surface is aflame. This occurred right after ignition of the sample. In Figure 31b char has begun to form creating a protective layer over the virgin wood underneath. Thus, the burning process slows down and HRR decreases. The second PHRR is seen in Figure 31c, the flames become more intense and appear in and around the cracks of the char. Figure 31d shows the sample after the second PHRR, the burning is slow, and the sample begins to glow and expand. Ash is also produced on the surface.

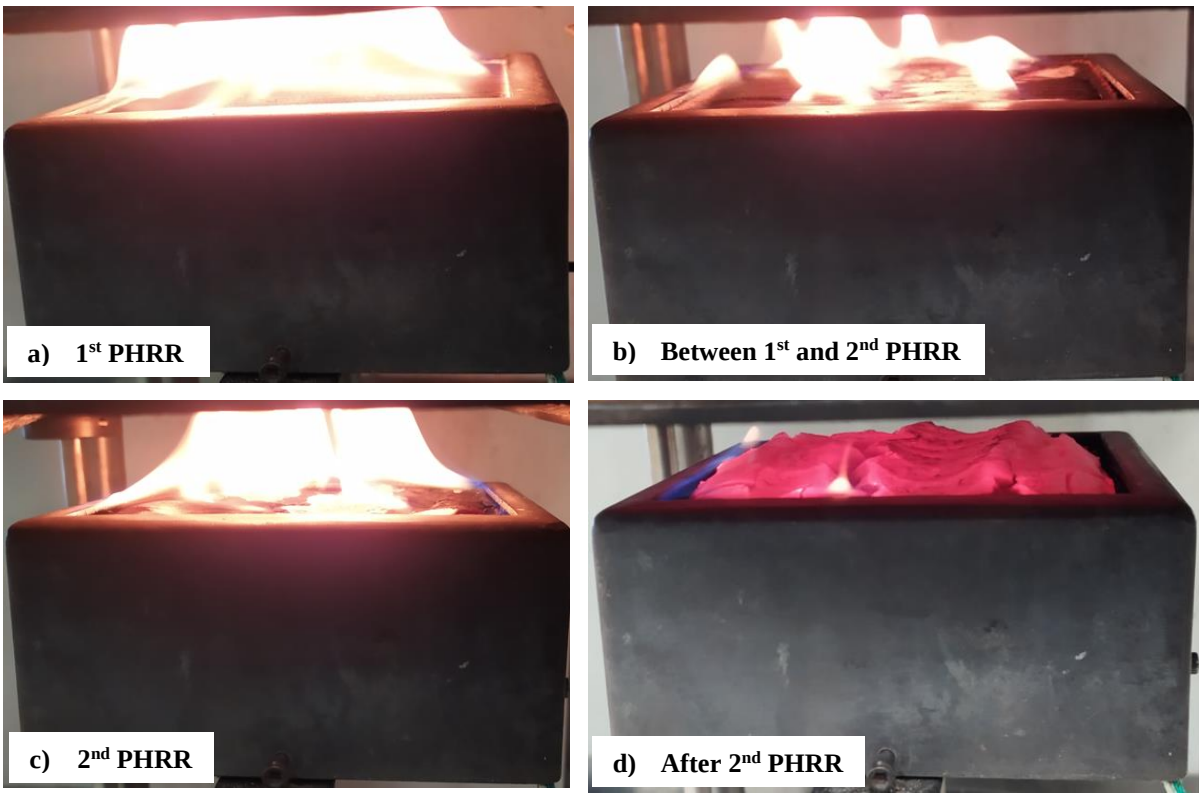

Figure 31. Burning process of a 10 mm sample with kaowool on the rear side of the sample. a) first PHRR, b) char forms and HRR decreases between the first and second peak, c) second PHRR and d) slow burning and glowing of sample after the second PHRR.

Figure 32a-b presents 10 and 30 mm samples with kaowool on the rear side immediately after removal from the cone calorimeter. A layer of ash has formed on the surfaces and the 30 mm sample has a thicker ash layer as well as larger and deeper cracks. Figure 322c-d show the rear side of the samples after flameout and cooldown. Both samples were fragile and had experienced burn through.

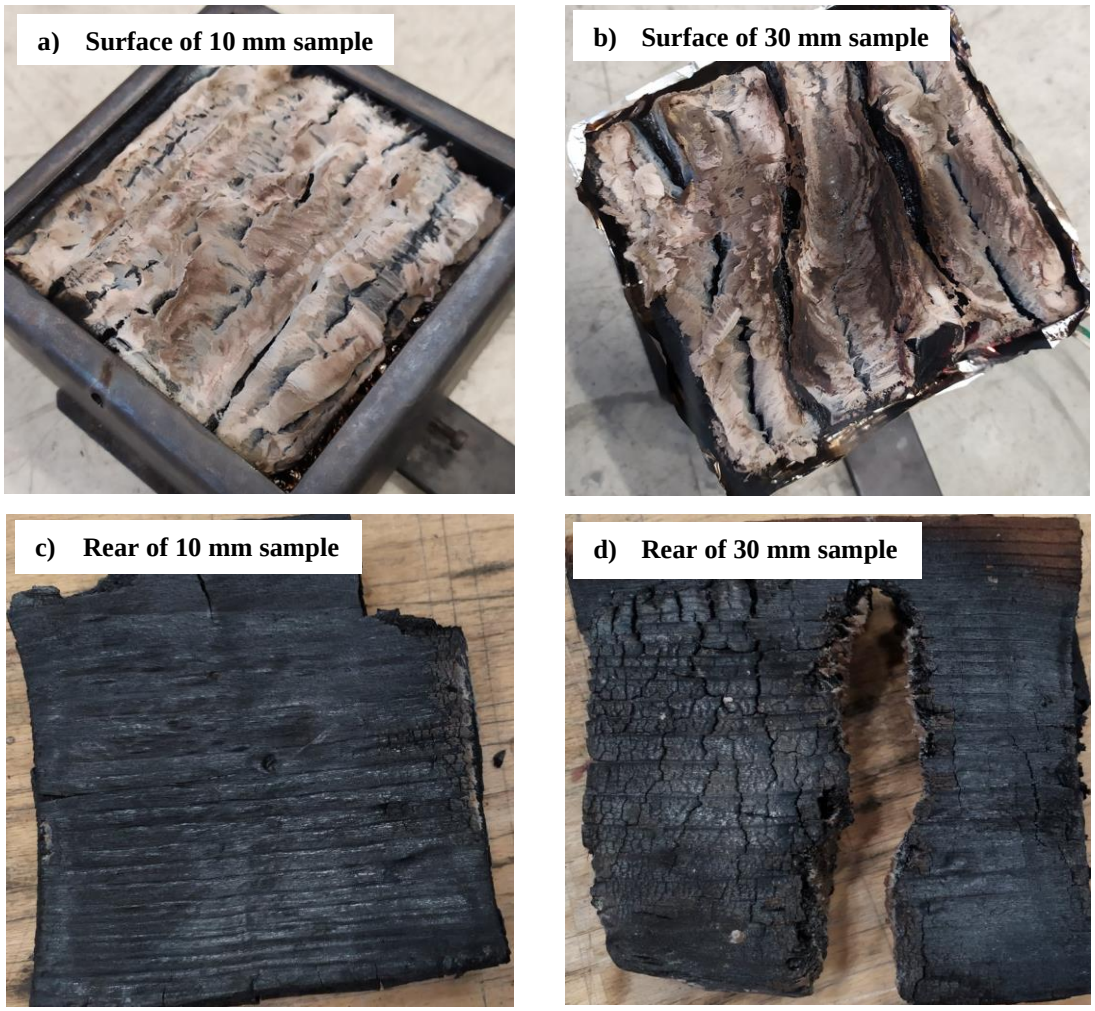

Figure 32. 10 and 30 mm samples with kaowool on the rear side after flameout. a) 10 mm sample after removal from the cone calorimeter, b) 30 mm sample after removal from the cone calorimeter, c) rear side of 10 mm sample and d) rear side of 30 mm sample.

4.1.2 Steel plate

Wood samples of 10 and 30 mm were tested with steel plates on the rear side of the samples. Three 10 mm samples each were tested with each steel plates of 8 and 20 mm thickness and three 30 mm samples were tested with an 8 mm steel plate according to Table 1. Ignition of the samples occurred around 25-40 s. Similar to the kaowool samples, the difference in ignition time might be due to a natural variation between the samples or slight warping towards or away from the cone heater (Spearpoint & Quintiere, 2001). It could also be an effect from a small divergence in distance between the cone heater and the samples. The samples were tested until flameout and Figure 33 presents the mean value (the prominent curves) and standard deviation (the shaded regions around the curves) of the sample HRR.

The initial peak of the 10 mm samples occurred at 55 (8 mm steel plate) and 40 s (20 mm steel plate) with HRR of 170 and 207 kWm^{-2} respectively. The peak of the 30 mm samples occurred at 45 s with an intensity of 191 kWm^{-2} according to Figure 33. The 10 mm samples with an 8 mm steel plate experienced a second peak at 430 s with HRR of 83 kWm^{-2}. The 10 mm samples with 20 mm steel plate and the 30 mm samples showed no indication of a second peak but instead a constant decrease in HRR throughout the analysis.

Similar to the temperature curves of kaowool, Figure 34 shows the temperature curves of the one sample closest to the mean value for each set of tests. All the temperatures can be seen in Appendix B – Steel plate. According to Figure 34, the highest temperature of 429 °C is experienced by the 10 mm sample with 8 mm steel on the rear side. The quickest flameout and lowest temperature of 97 °C is attained by the 10 mm sample with 20 mm steel. The 30 mm sample also experienced a relatively low maximum temperature of 224 °C.

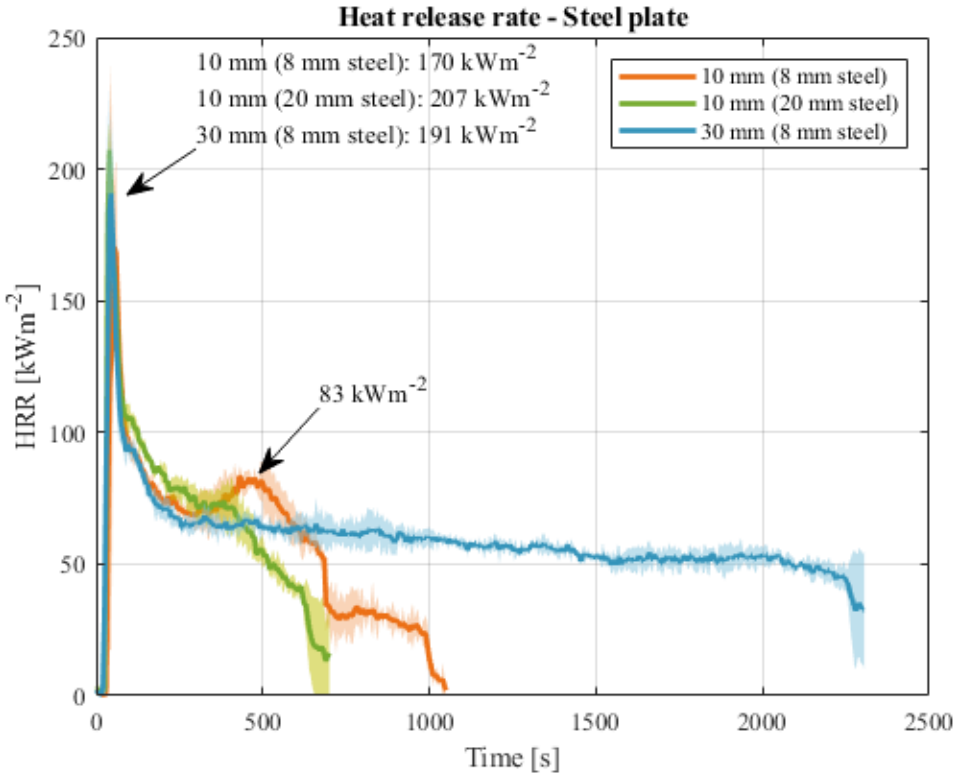

Figure 33. Mean value of HRR as a function of time for 10 and 30 mm wood samples with a steel plate on the rear side. Standard deviation is calculated and is represented by the shaded area.

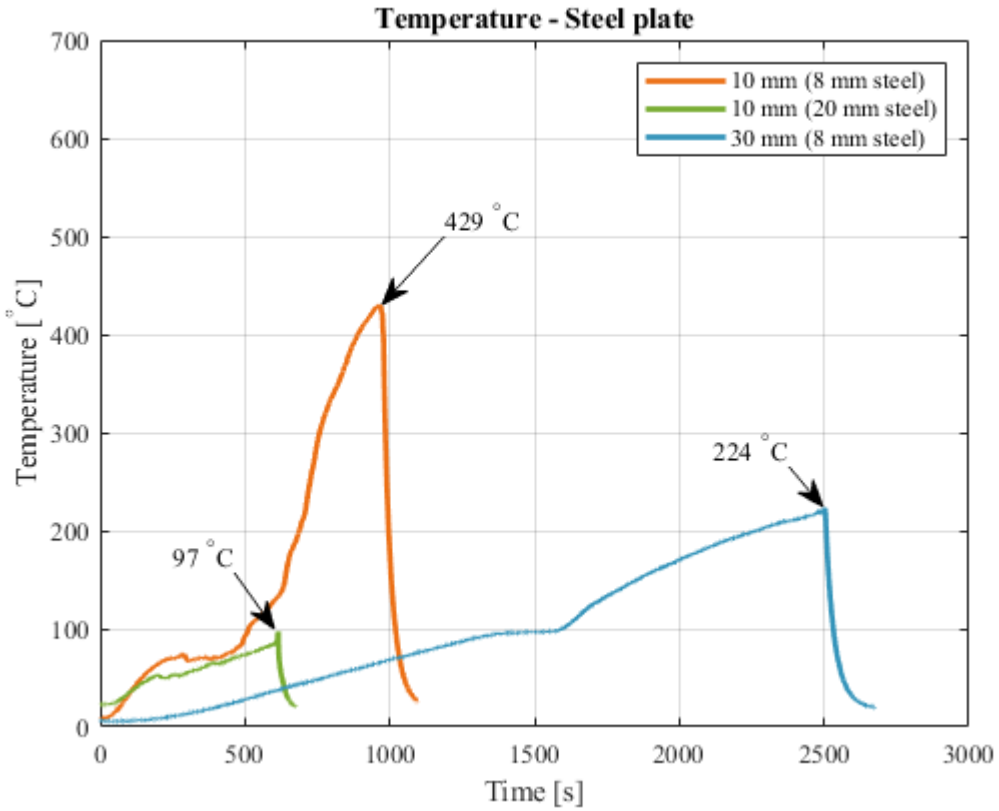

Figure 34. Temperature as a function of time for 10 mm samples with 8 and 20 mm steel plate and 30 mm samples with an 8 mm steel plate on the rear side. Each curve represents one sample of each sample composition.

Figure 35a-c presents the rear side of the 10 and 30 mm samples after flameout. The 10 mm sample with 8 mm steel plate seen in Figure 35a is almost completely burnt while Figure 35b, representing the 10 mm sample with 20 mm steel, only shows limited signs of charring. The 30 mm sample, see Figure 35c, is similar to Figure 35b as it still shows fresh wood and only signs of charring at the corners of the rear side.

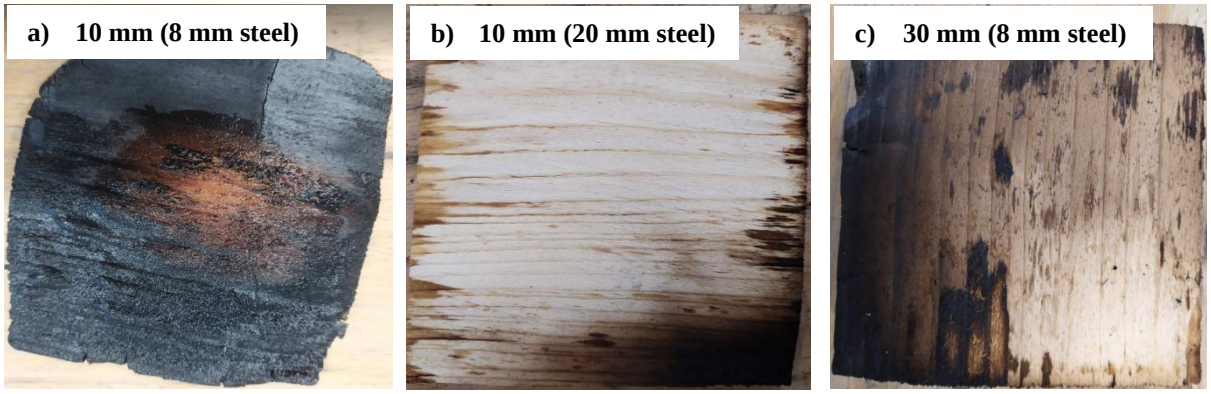

Figure 35. Rear side of wood samples after flameout. a) shows 10 mm sample with 8 mm steel plate, b) shows 10 mm sample with 20 mm steel plate and c) shows 30 mm sample with 8 mm steel plate.

4.1.3 Aluminium foil around wood

Wood samples of 10 and 30 mm were tested with aluminium foil wrapped around a piece of wood (100x100x10 mm) on the rear side of the sample. This was done to provide the same thermal properties as normal wood but for no further combustion to take place. The ignition time of the different samples varied between 35-40 s, this may be due to a natural variation between the wooden samples or by slight warping of the samples (Spearpoint & Quintiere, 2001). Furthermore, a small difference in distance between the cone heater and samples might also affect the result. The samples were tested until flameout and Figure 36 presents the mean value (the prominent curves) and standard deviation (the shaded regions around the curves) of the calculated HRR. The HRR curve for 10 mm is represented by all three tested samples while the 30 mm is represented by two samples as one sample deviated significantly from the others.

According to Figure 36 the initial peak of the 10 mm samples occurred at 50 s with HRR of 187 kWm^{-2} and the 30 mm samples at 40 s with HRR of 204 kWm^{-2}. The 10 mm samples reached the highest second PHRR of 122 kWm^{-2} at 460 s. There is no steep second peak for the 30 mm samples but instead a slow-rising curve with a maximum HRR of 88 kWm^{-2} at 1845 s.

Figure 37 shows temperature curves of 10 and 30 mm samples. All samples in one set of tests experienced divergence in temperature, therefore it was not possible to create a mean value of all samples. Hence, Figure 37 presents the temperature curve of the samples closest to the mean value of each sample combination. Remaining temperature curves can be seen in Appendix C – Aluminium foil wrapped around wood. It is observed that the 30 mm sample attain a slower but higher temperature rise than the 10 mm sample with a maximum temperature of 670 °C. The 10 mm sample has a quicker temperature rise with maximum temperature of 445 °C.

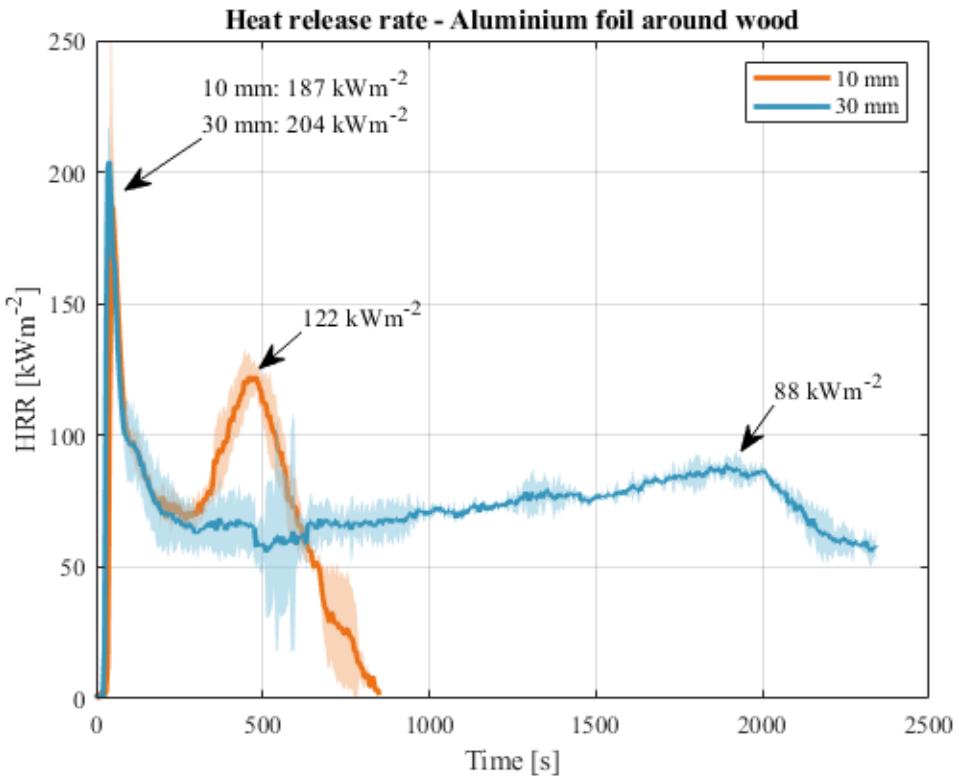

Figure 36. Mean value of HRR as a function of time for 10 and 30 mm wood samples with aluminium foil wrapped around a piece of wood placed on the rear side of the sample. Standard deviation is calculated and shown by the shaded area.

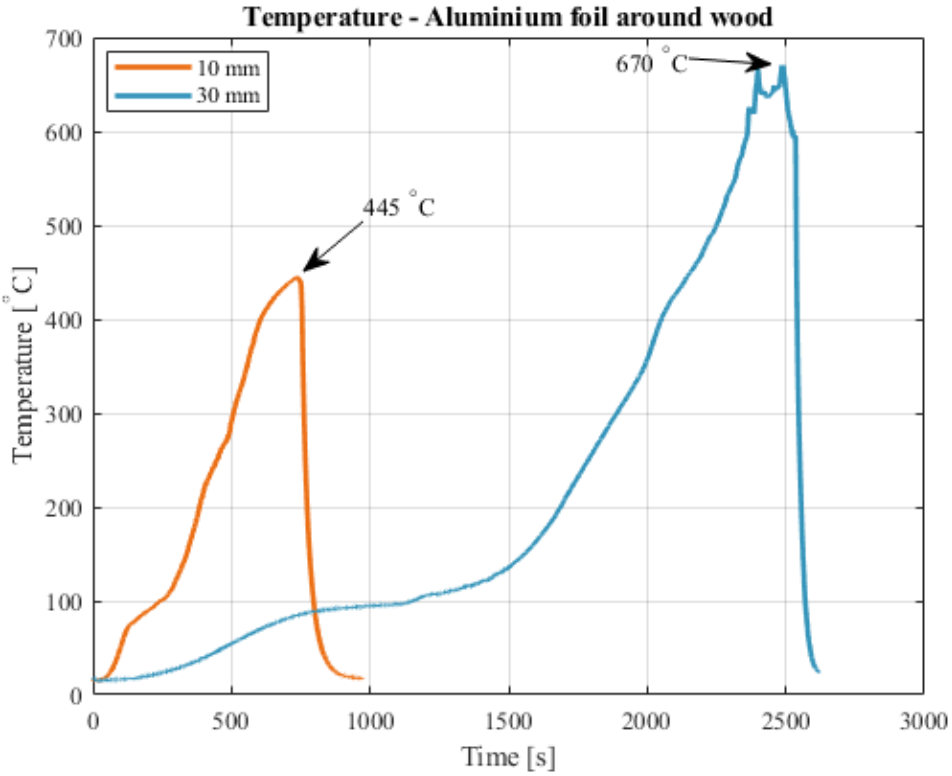

Figure 37. Temperature as a function of time for 10 and 30 mm wood samples with aluminium foil wrapped around wood on the rear side. Each curve represents one sample of each sample composition.

The rear side after flameout and cooldown of a 10 and 30 mm sample with aluminium foil wrapped around wood on the backside can be seen in Figure 38a-b. It is observed that the samples are completely burnt showing no signs of virgin wood. They are also fragile with relatively large cracks.

Figure 38. Rear side of samples with aluminium foil wrapped around wood on the backside after flameout. a) 10 mm sample and b) 30 mm sample.

4.1.4 Effects of rear material

Figure 39 presents a compilation of HRR from the 10 mm wood samples tested with different rear materials, namely kaowool, steel and aluminium foil wrapped around a piece of wood. The initial and second peaks occurred at approximately the same time of 50-55 s and 430-460 s respectively. All samples except the samples with a 20 mm steel plate experienced a second PHRR. According to Figure 39, kaowool used as rear material provided the highest second peak of 160 kWm^{-2} and the 8 mm steel plate, the lowest of 83 kWm^{-2}. This produces a large difference in HRR of 77 kWm^{-2} between the two. Aluminium foil wrapped around wood contributed with a relatively high second HRR peak of 122 kWm^{-2}, however it is not as high as that of kaowool with a difference of 38 kWm^{-2}.

The temperature curves of the 10 mm samples can be seen in Figure 40. Kaowool had the quickest and highest temperature rise with a maximum of 560 °C. The samples with 8 mm steel plate and aluminium foil wrapped around wood reached almost the same temperature with a difference of 16 °C, however, the steel plate experienced its maximum temperature around 220 s after the sample with aluminium foil wrapped around wood. The lowest temperature of 97 °C is attained by the sample with a 20 mm steel plate.

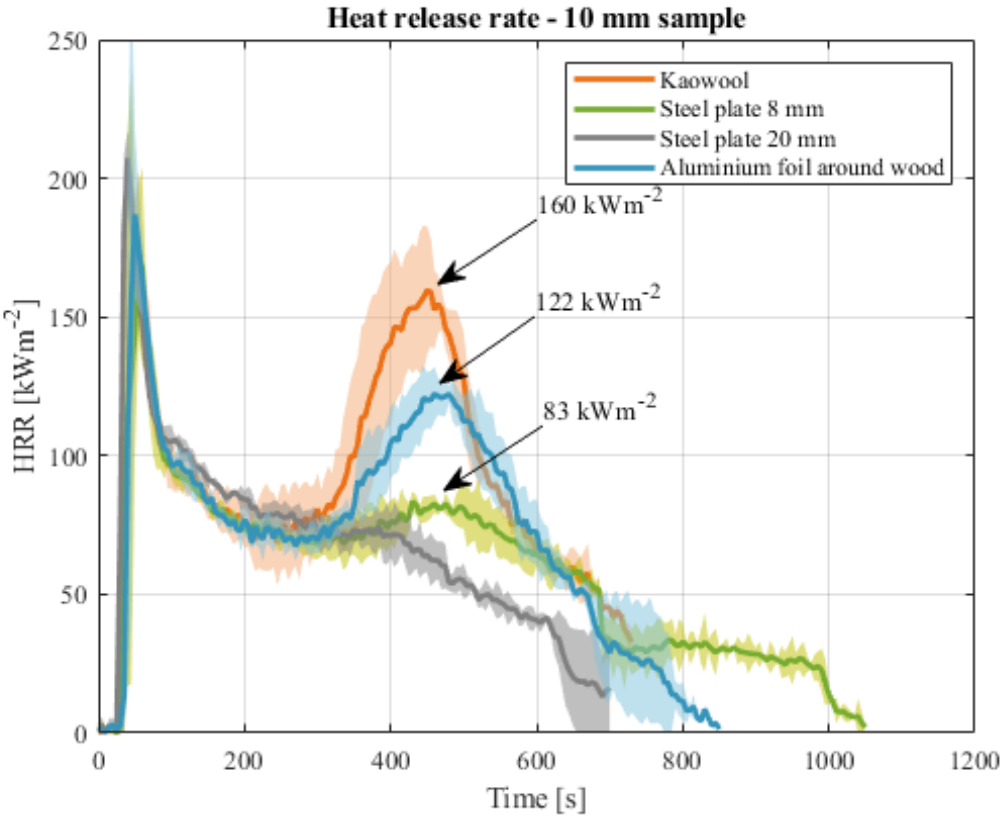

Figure 39. Mean value of HRR as a function of time for 10 mm samples with kaowool, steel and aluminium foil around wood on the rear side. Standard deviation is shown by the shaded area.

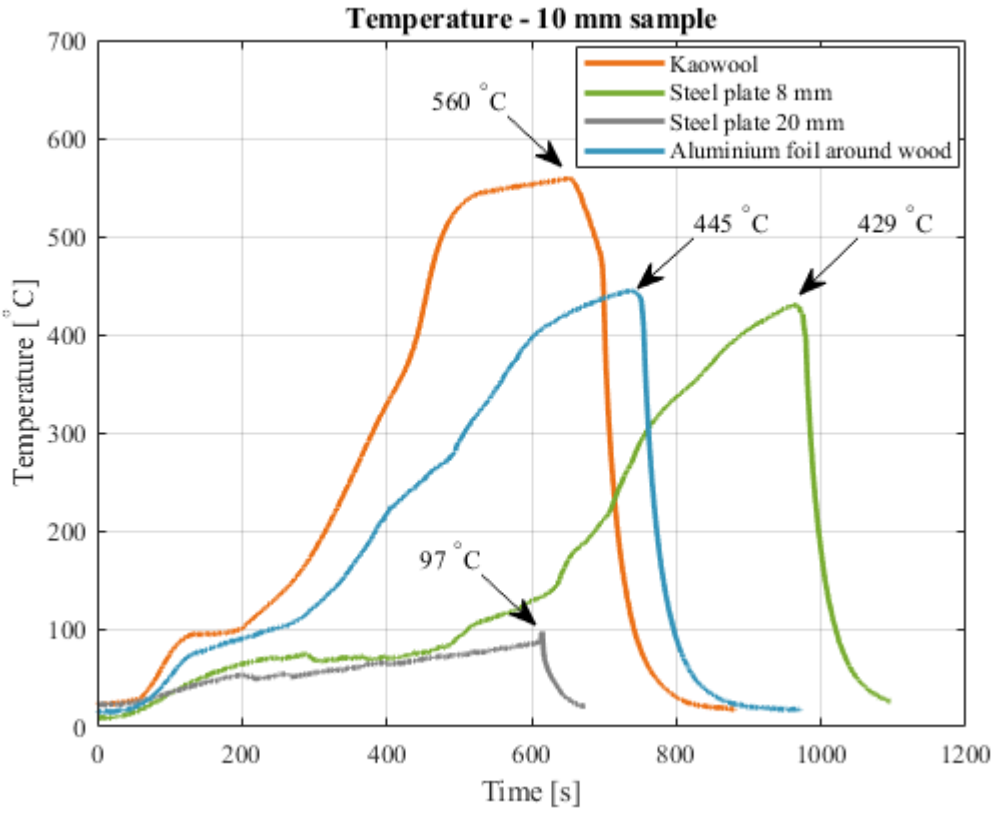

Figure 40. Temperature as a function of time for 10 mm samples with kaowool, steel plate and aluminium foil around wood on the rear side.

The initial PHRR for the 30 mm samples appears at 30-40 s and the second peak at 1800-1900 s, seen in Figure 41. All curves except the steel plate had a second PHRR. The curve of aluminium foil wrapped around wood had the highest second peak of 88 kWm^{-2} closely followed by kaowool of 78 kWm^{-2}.

Figure 42 shows the temperature curves of the 30 mm samples. The curve of aluminium foil wrapped around wood experienced the highest maximum temperature of 670 °C. The second highest temperature is that of kaowool with a temperature of 530°C and the lowest is the steel plate of 224 °C. All samples reached their maximum temperature around the same time of 2400-2500 s. However, the maximum temperature differs between the samples. The difference between kaowool and aluminium foil is 140 °C and the difference between kaowool and the steel plate is 306 °C.

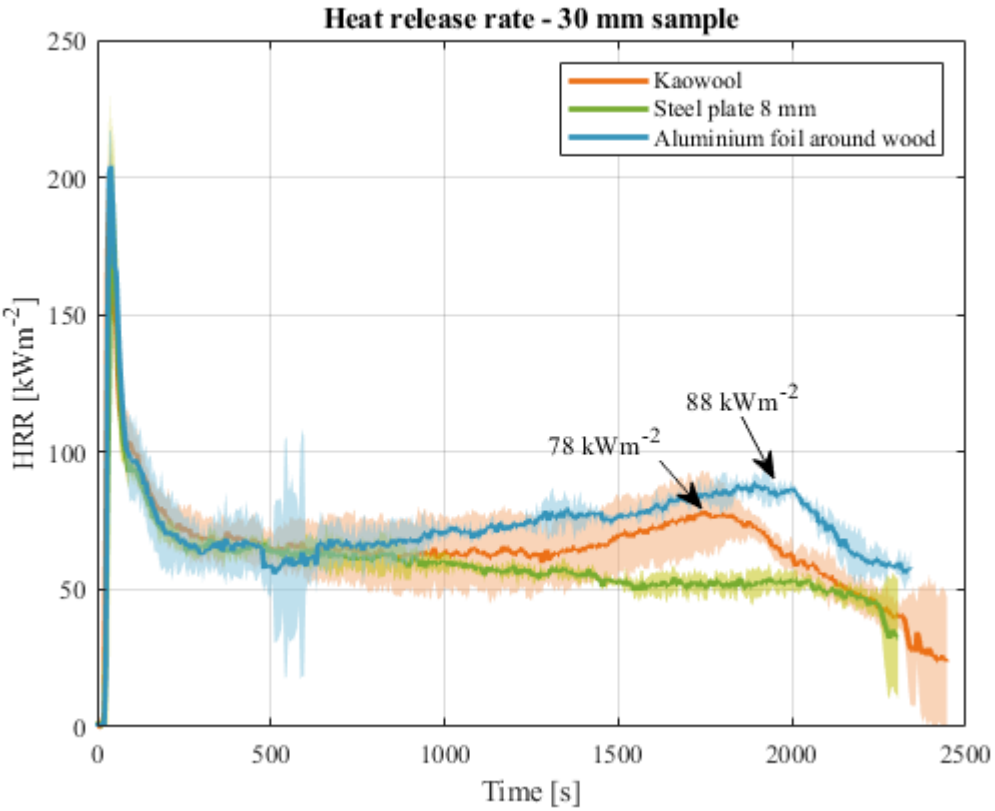

Figure 41. Mean value of HRR as a function of time for 30 mm samples with kaowool, steel plate and aluminium foil around wood on the rear side. Standard deviation is shown by the shaded area.

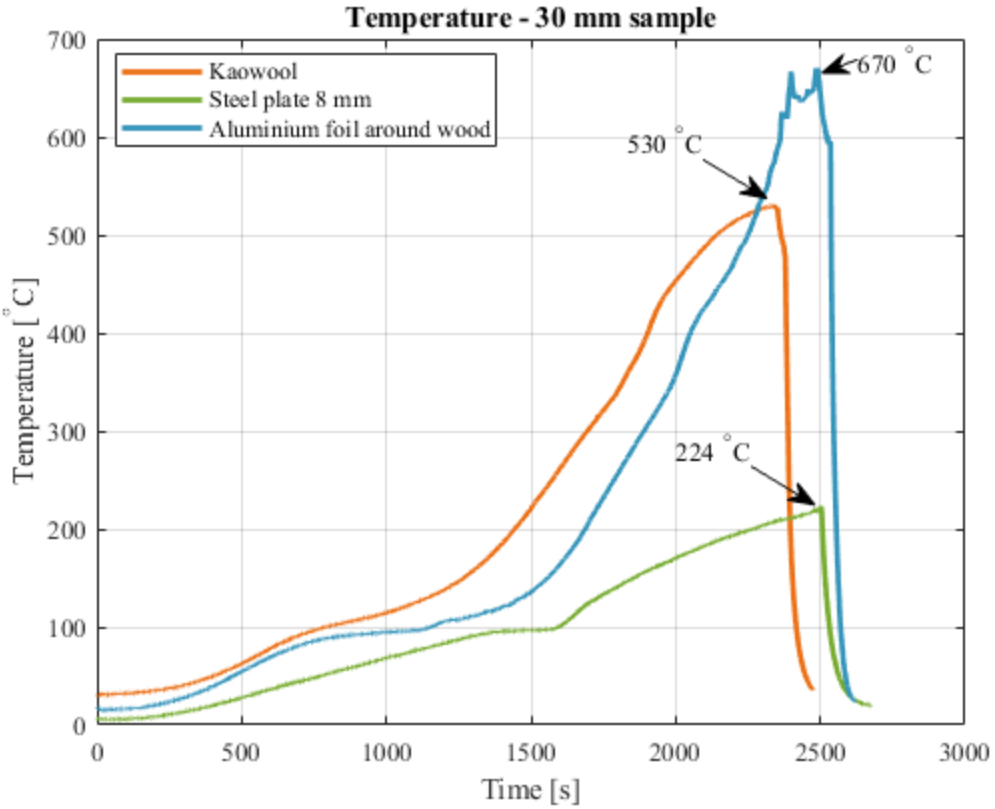

Figure 42. Temperature as a function of time for 30 mm samples with kaowool, steel plate and aluminium foil around wood on the rear side.

4.1.5 Moisture content vs. sample thickness

In order to analyse the effect of moisture on HRR, samples of 10, 20 and 30 mm with moisture ratios ranging from 11.2-20.8 %, were dried at 100 °C for over one week, to attain a moisture ratio of 5-8 %. The samples were tested in the cone calorimeter, with kaowool on the rear side, until flameout and HRR was measured, see Figure 43 showing mean value and standard deviation. The 10 and 30 mm HRR curves are represented by three samples while the 20 mm curve is represented by two samples as one sample deviated significantly from the rest. Ignition of the sample surface occurred around 20-35 s and all tests reached the initial PHRR around 35-45 s with intensities of 214-246 kWm^{-2}. Thereafter, the HRR decreased as char formed. Similar to previous performed tests it is shown that the 10 mm sample's curve acquired the highest and quickest second PHRR of 179 kWm^{-2} at 325 s. However, the 30 mm sample's curve show both a second and third peak which is not seen with any other sample. Both peaks reached similar HRR of 128 and 122 kWm^{-2} at 265 and 850 s, respectively. The second PHRR of the 20 mm samples occurred around 670 s with an intensity of 126 kWm^{-2}, which lies between the second and third PHRR of the 30 mm samples. Moreover, out of the three tested 30 mm samples only two showed a second and third peak, the 30 mm mean value HRR curve seen in Figure 43 is a combination of all three tests.

The samples during analysis reached around the same maximum temperature, seen in Figure 44 where the temperature curves are represented by one sample of each thickness. All temperature curves can be seen in Appendix D – Low moisture content. The 10 mm sample reached a maximum of 492 °C at 550 s, the 20 mm sample reached 495 °C at 880 s and the 30 mm sample reached 476 °C at 1403. This indicates that the time for flameout increases exponentially with a thicker sample.

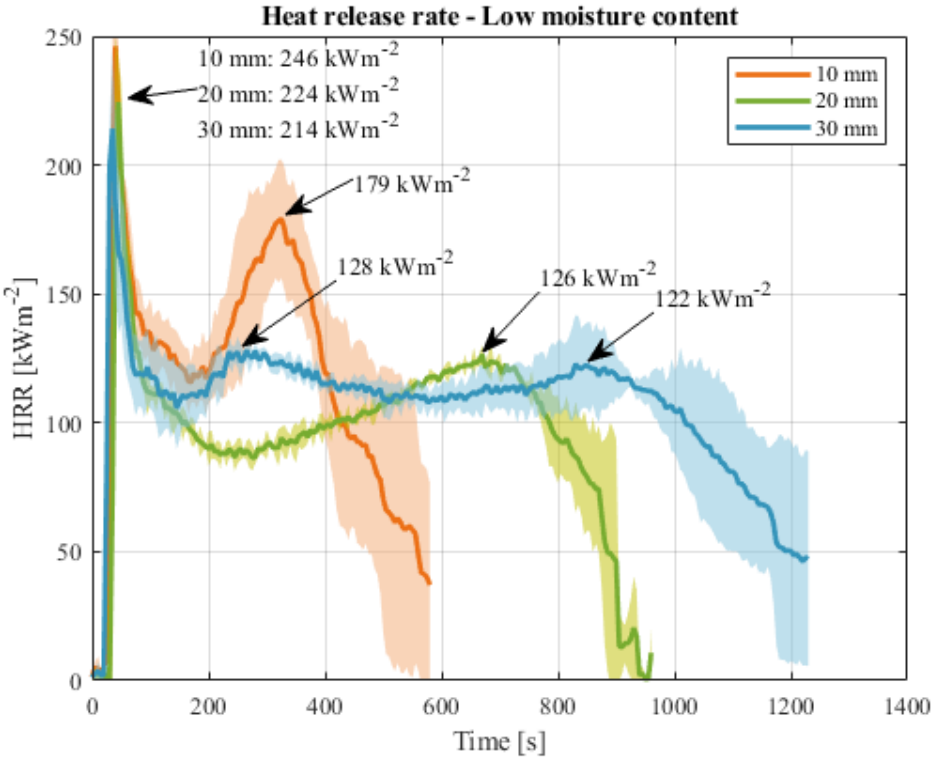

Figure 43. Mean value of HRR as a function of time for 10, 20 and 30 mm low moisture content samples. Standard deviation is shown by the shaded area.

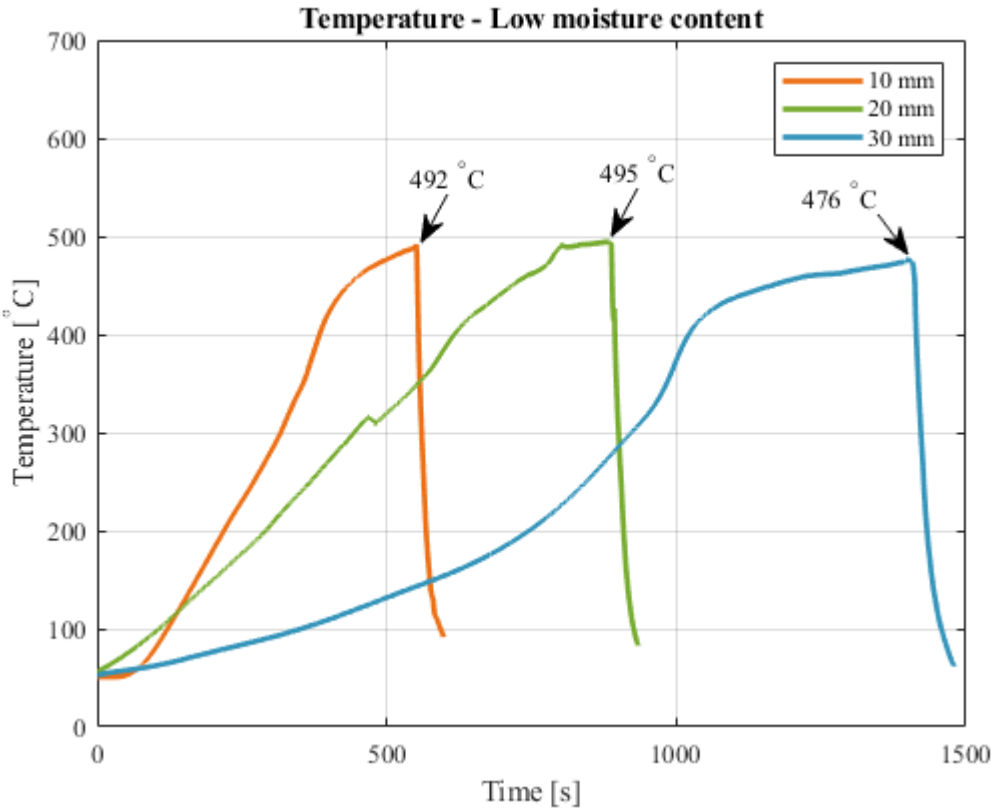

Figure 44. Temperature as a function of time for 10, 20 and 30 mm low moisture content samples. Each curve is represented by one sample of each thickness.

Figure 45a-c presents the rear side of 10, 20 and 30 mm samples after flameout and cooldown. All samples were fragile and completely charred. The 30 mm sample was the most fragile, which fell apart and crumbled almost immediately.

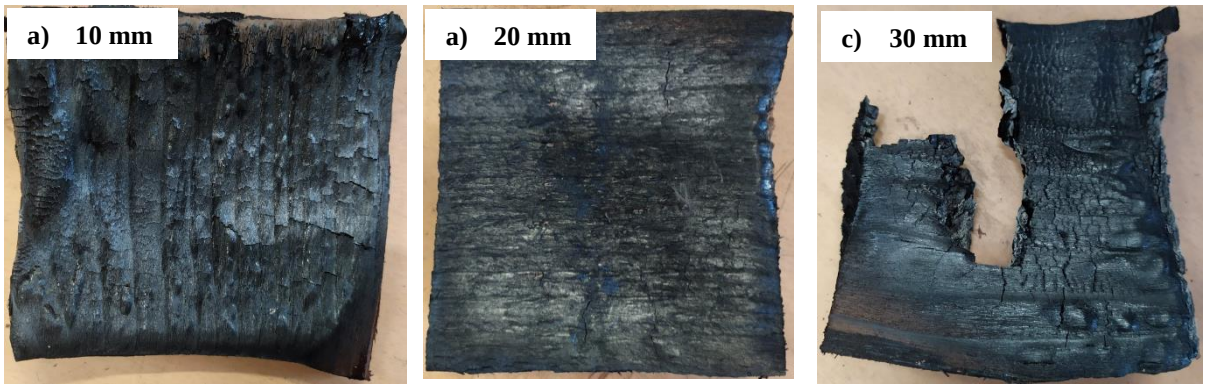

Figure 45. Rear side of low moisture content samples after flameout and cooldown. a) 10 mm sample, b) 20 mm sample and c) 30 mm sample.

Figure 46 shows a compilation of all kaowool tests with normal (wet) and low (dry) moisture contents. 10 and 30 mm dry samples approached flameout faster than their correspondent wet samples and also had higher PHRR. However, this is not seen between the 20 mm dry and wet samples where the wet samples experienced the higher second PHRR of the two and both occurred around the same time.

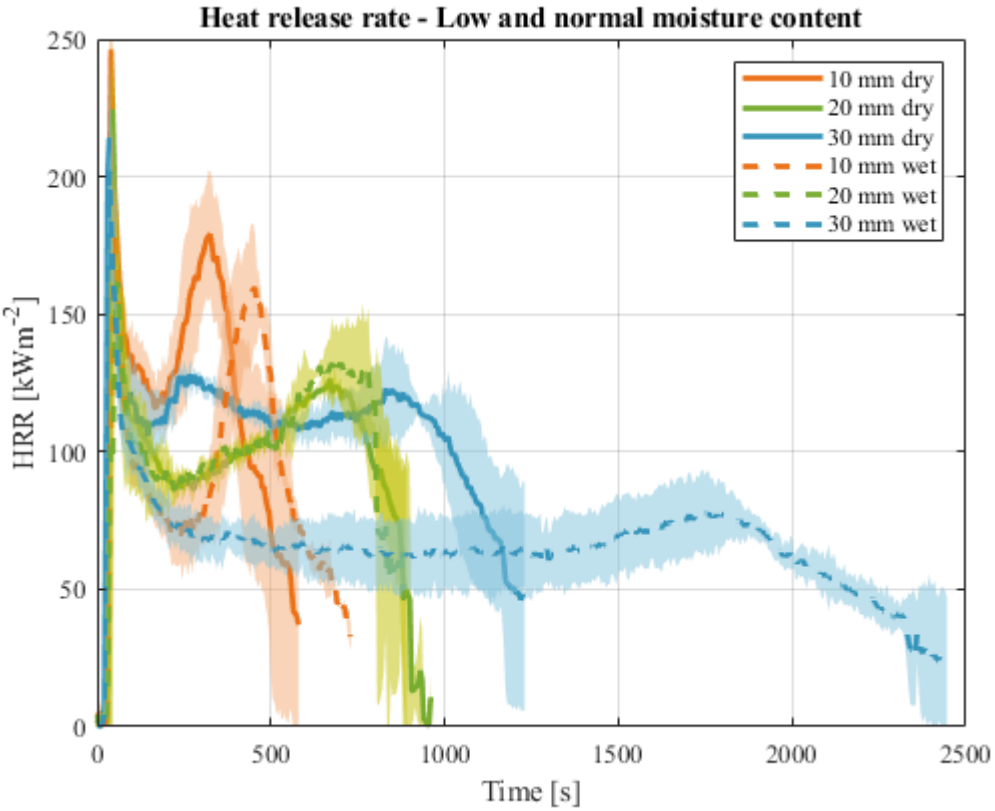

Figure 46. Mean value of HRR as a function of time for 10, 20 and 30 mm normal (wet) and low (dry) moisture content samples. Standard deviation is showed by shaded area.

Table 4 shows the difference in time and PHRR between the wet and dry wood samples (calculated as $PHRR_{dry} - PHRR_{wet}$ and $Time_{PHRR,dry} - Time_{PHRR,wet}$). The initial peaks appear around the same time for all samples. However, the HRR of the dry samples is more intense than the wet samples. The second PHRR is greatly prolonged for 10 and 30 mm samples but not for the 20 mm samples where the peaks appear with a 15 s difference. The wet wood also experiences an 8 kWm^{-2} higher PHRR than the dry wood at this point, which is the opposite of other thicknesses. 30 mm dry wood reach both a second and third PHRR, however the latter is not achieved by wet wood.

Table 4. Difference in PHRR and time between normal (wet) and low (dry) moisture content samples, calculated $PHRR_{dry} - PHRR_{wet}$ and $Time_{PHRR,dry} - Time_{PHRR,wet}$.

Sample thickness	Difference between initial peaks		Difference between second peaks	
	PHRR [kWm^{-2}]	Time [s]	PHRR [kWm^{-2}]	Time[s]
10 mm	68	- 10	19	- 125
20 mm	63	- 15	- 8	- 15
30 mm	12	0	44 (2^{nd} wet and 3^{rd} dry peak)	- 890 (2^{nd} wet and 3^{rd} dry peak)

4.2 Progression of char zone

The following section presents an analysis of the char zone progression during the second PHRR of samples with kaowool and 8 mm steel plate on the rear side.

4.2.1 Kaowool

To analyse the char progression during the second PHRR three samples of 10 and 20 mm were tested with kaowool in the cone calorimeter. The samples were removed prior to, at and after the second peak. 30 mm samples were not analysed as the second PHRR on these samples were less defined and hence difficult to "catch".

Figure 47a-c shows the progression of the char zone during the second peak for 10 mm wood samples. The char zone before the peak at around 280 s can be seen in Figure 47a, the char layer has reached the middle of the sample and beneath the layer of char is fresh virgin wood. Figure 47b presents the progression of the char zone at the second PHRR, roughly around 420 s. It is observed that the wood has almost experienced burn through. Figure 47c shows the wood sample after the second peak at around 520 s. No fresh wood is remaining, and the sample is completely burnt with brittle structure and ash showing on the sample surface.

Over time the creation of char proceeds further into the wood sample, cracks appear early and grows wider and deeper as the char layer becomes thicker. Moreover, the sample deforms gradually as the char layer enlarges, this is seen in Figure 47c where the sample has been bent upwards.

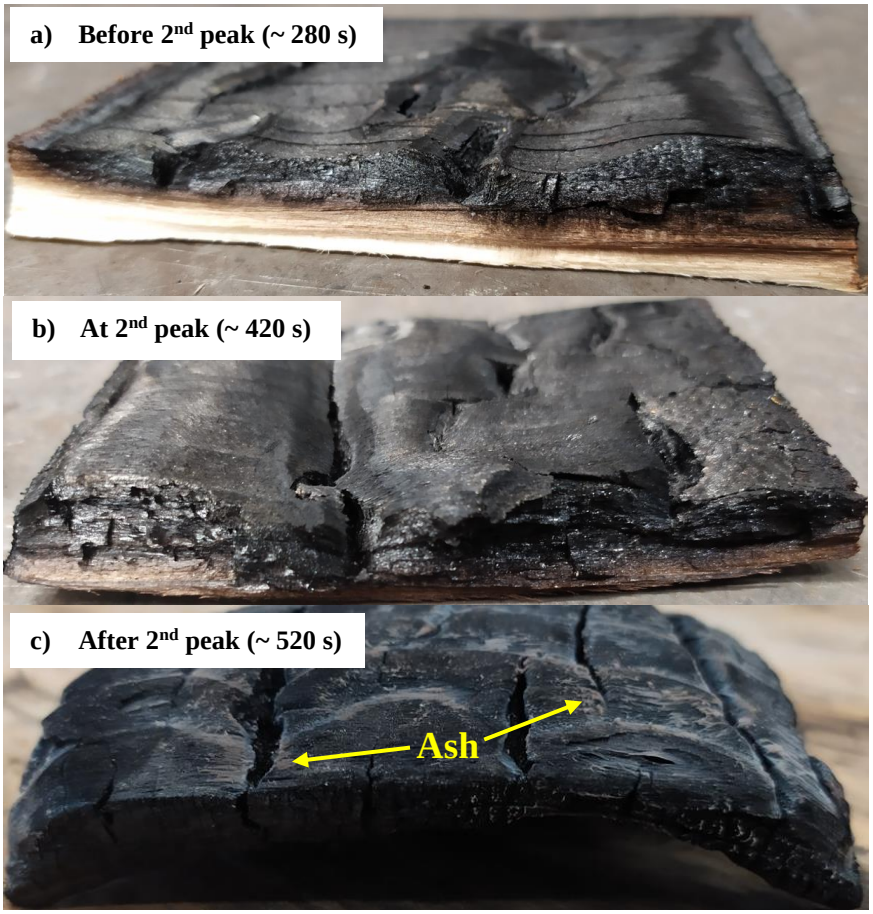

Figure 47. Char progression during the second PHRR for 10 mm wood sample. a) before second peak, b) at second peak and c) after second peak.

The progression of the char zone in 20 mm samples is seen in Figure 48a-c, which has a similar trend to that of the 10 mm samples. Prior to the second PHRR, around 580 s, the char layer is approaching the middle of the sample, see Figure 48a. The char progression at the peak around 760 s can be seen in Figure 48b, the sample has almost experienced burn through. After the second PHRR at 850 s, seen in Figure 48c, it is revealed that the sample is completely burnt with large cracks and ash formation on the sample surface.

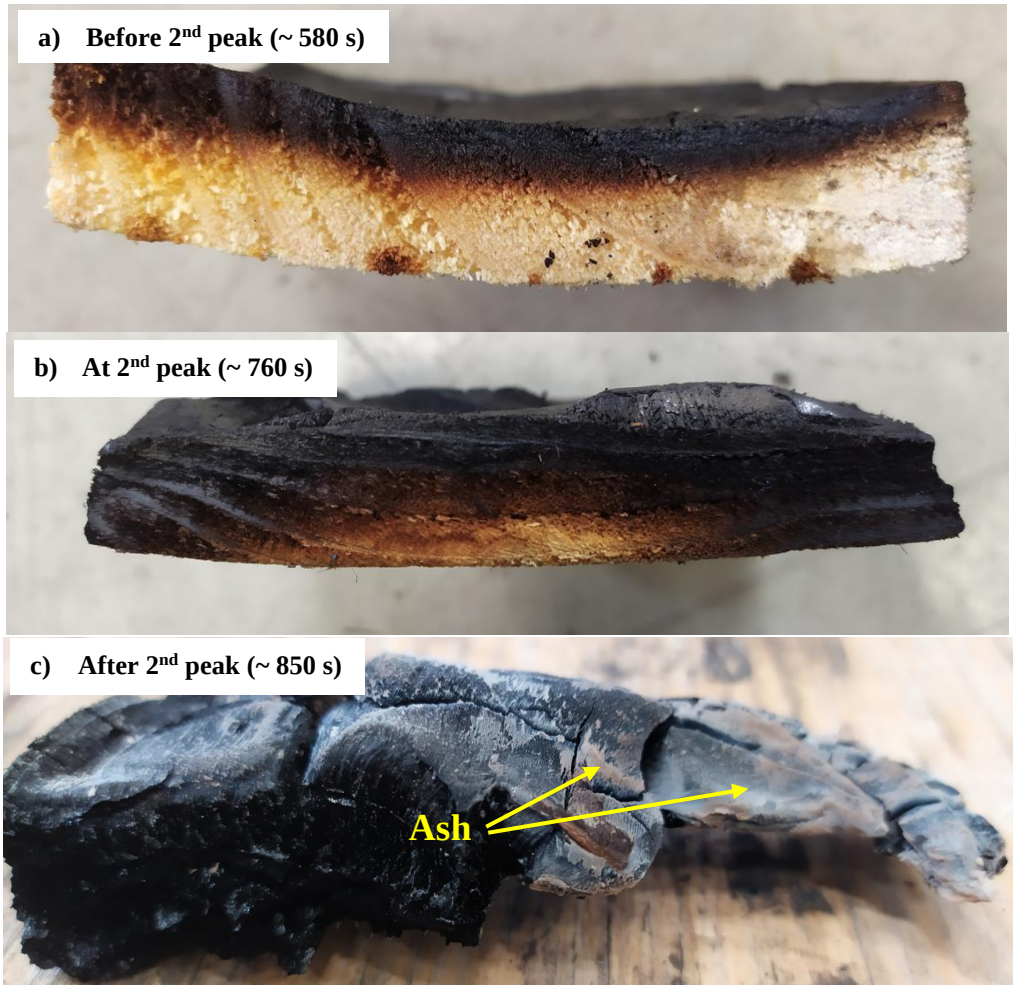

Figure 48. Char progression during the second PHRR for 20 mm wood sample. a) before second peak, b) at second peak and c) after second peak.

The char progression during the second PHRR in 10 and 20 mm samples are similar, both samples experience a char zone close to the sample centre prior to the second peak. Both samples are almost burnt through at the second peak and by the end of the peak they are completely burnt. However, wider and deeper cracks can be observed in the 20 mm sample as well as an increased production of ash compared to the 10 mm sample.

4.2.2 Steel plate

Similar to section 4.2.1, 10 mm samples were tested with an 8 mm steel plate and removed at multiple timesteps throughout the second PHRR. This was done to gain a better understanding about the occurrence of a second peak on these samples and why it does not occur on the other sample combinations with steel plates, seen in Figure 35a-c. The second peak occurs around 430-460 s, hence the tests were stopped at 440, 460, 490 and 780 s seen in Figure 49a-d. Figure 35a shows that the 10 mm sample with 8 mm steel is almost completely burnt by the end of analysis while the other samples only show some charring at the corners. Therefore, Figure 49a-d show photos of the rear side of the samples so that they can be compared to Figure 35a-c.

There is not a big difference between Figure 49a-c, which represent a timespan over the second peak. However, it is observed that the charring has started to reach the rear side of the sample during this period of time. At 780 s, Figure 49d, the charring has grown larger but has not yet covered the entire sample backside.

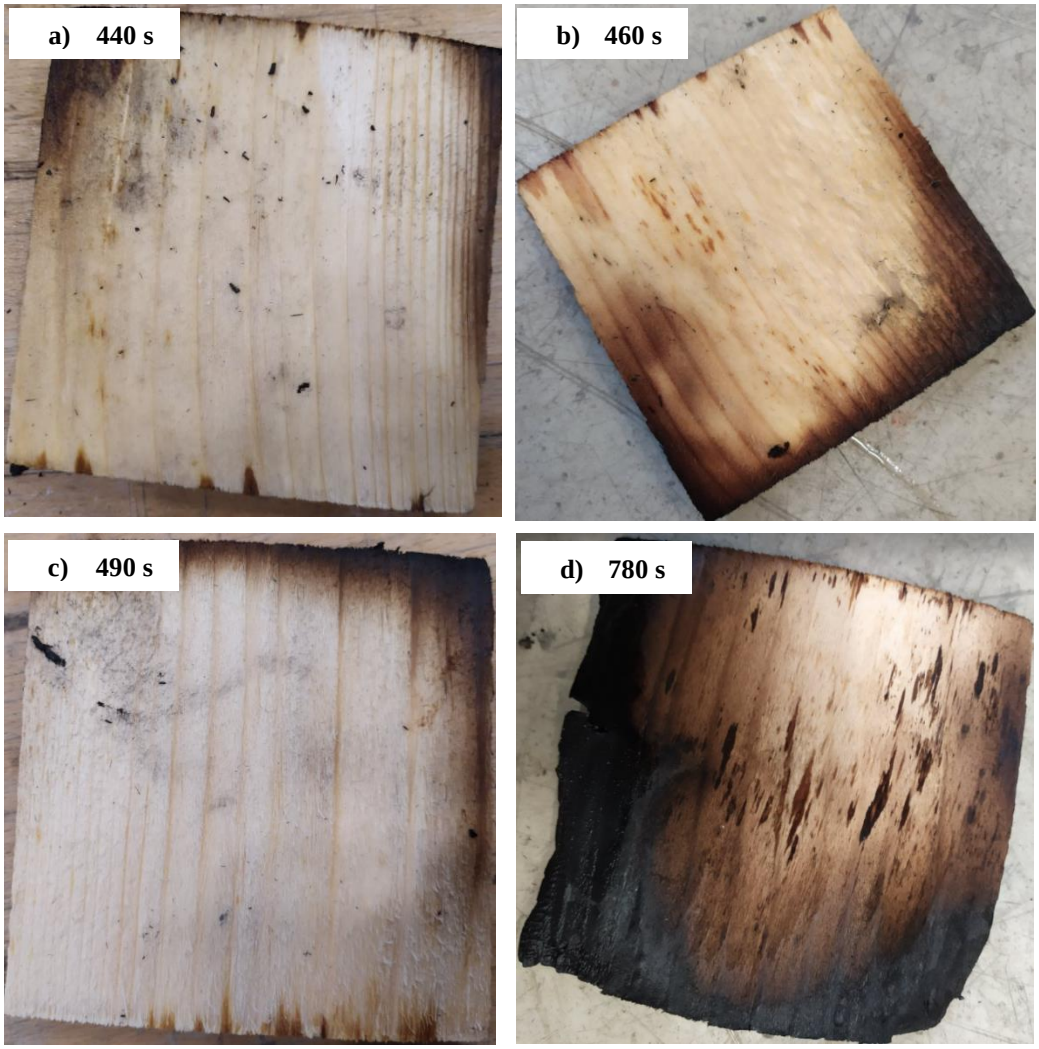

Figure 49. Char progression at different timesteps of the second PHRR of 10 mm samples with an 8 mm steel plate on the rear side. a) at 440 s, b) at 460 s, c) at 490 s and d) at 780 s.

4.3 Moisture transport

Moisture transport through 10, 20 and 30 mm wood samples with kaowool were analysed. Three samples were tested for each thickness and the results are shown as mean value (the prominent curves) and standard deviation (the shaded region surrounding the curves) of relative humidity in Figure 50. All samples were tested until the humidity sensor reached 60 °C, in order to protect the sensor, and as a result the humidity could not be measured during the entire burning process. It was observed that the highest humidity of 95 %RH was reached by the 10 mm samples. The curve had a steep rise from 50 s, which slowed down after 100 s, and at 150 s the curve rapidly increased again reaching its maximum relative humidity. The 20 mm samples had the second highest humidity of 65 %RH. The curve had a slower increase compared to the 10 mm samples and reached its maximum after 250 s. It was also observed that the humidity started to decrease around 275 s before it was removed from the cone calorimeter. The 30 mm samples had the lowest and slowest increase of humidity, reaching a maximum of 54 %RH at around 350 s. Similar to the 20 mm samples the curve showed an indication of decrement around 375 s before being removed from the cone calorimeter.

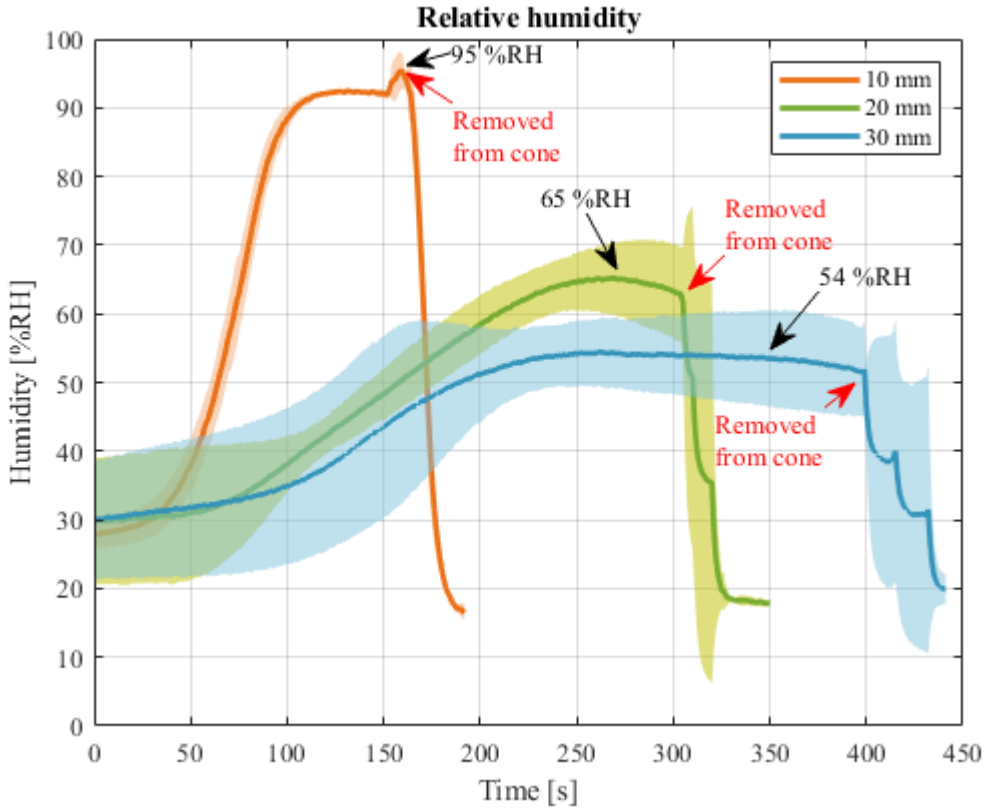

Figure 50. Mean value of relative humidity as a function of time for 10, 20 and 30 mm wood samples with kaowool on the rear side. Standard deviation is calculated and shown by the shaded area.

The samples when removed from the cone calorimeter is seen in Figure 51. The samples did not experienced burn through. The layer of char reached the deepest in the 10 mm sample meaning that the 20 and 30 mm sample had a larger wet zone (see Figure 20).

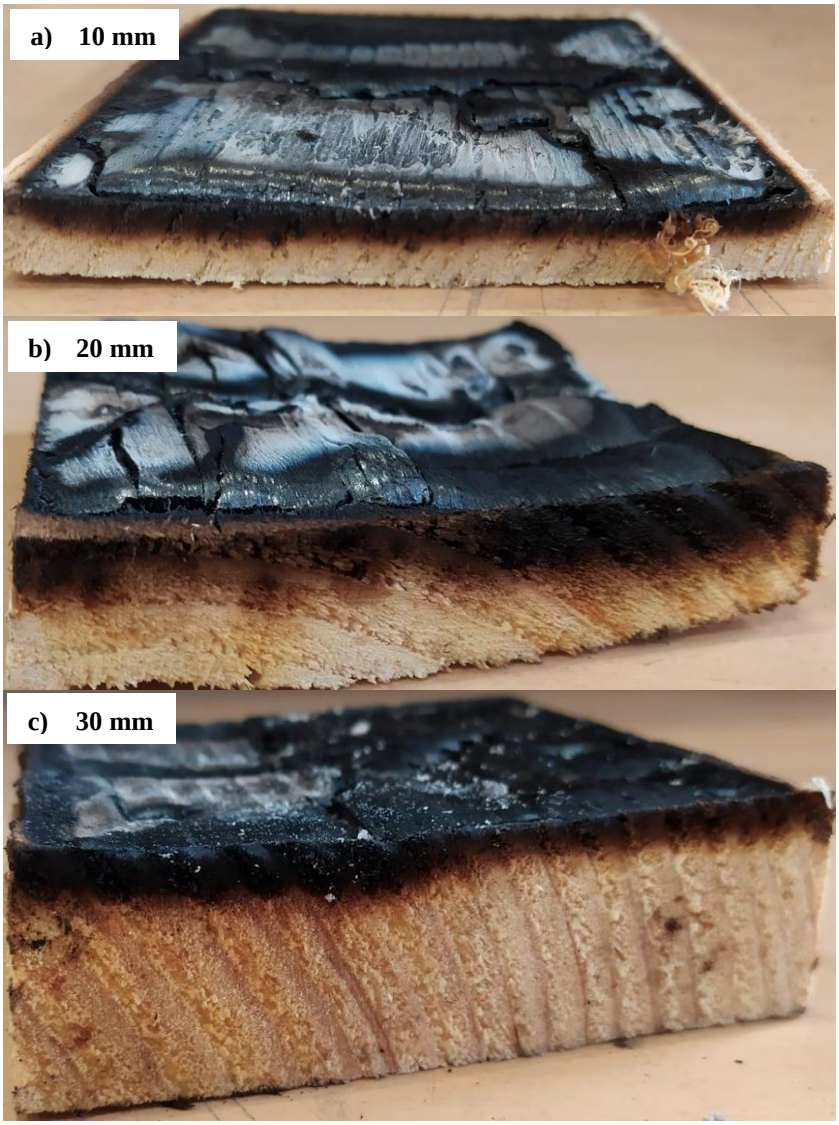

Figure 51. Samples after removal from the cone calorimeter. a) 10 mm, b) 20 mm and c) 30 mm.

4.4 Char microstructure

Figure 52 shows SEM images of pristine spruce wood and char after the cone calorimeter tests. Pristine spruce wood shows a porous structure with intact lumina and pits (Figure 52a). Spruce wood after the second PHRR, presented in Figure 52b shows that most of the wood microstructures are still intact, which is most likely due to the liquid nitrogen halting the combustion process. Additionally, char is known to retain the majority of the structure of the parent biomass, if the thermo-chemical conversion is pyrolytic in nature (Das et al., 2018). However, in Figure 52b, two major features are visible, white particle-like agglomerations and fibre-like layers on the edges of the cell lumens. According to Udoeyo et al. (2006) these agglomerations and fibres are ash generated from burning the wood sample. Spruce wood before and after the second PHRR are presented in Figure 52c-d. For the sample, after the second PHRR, the crack is at least three times larger than the sample before the second PHRR. The widening of the crack is attributed to the progression of heating that is known to cause expansion. The formation of wider cracks increases the surface area of the entire sample, which facilitates increased burning. Moreover, ash formation is observed on the sample surface after the second peak, seen as white interconnecting fibres.

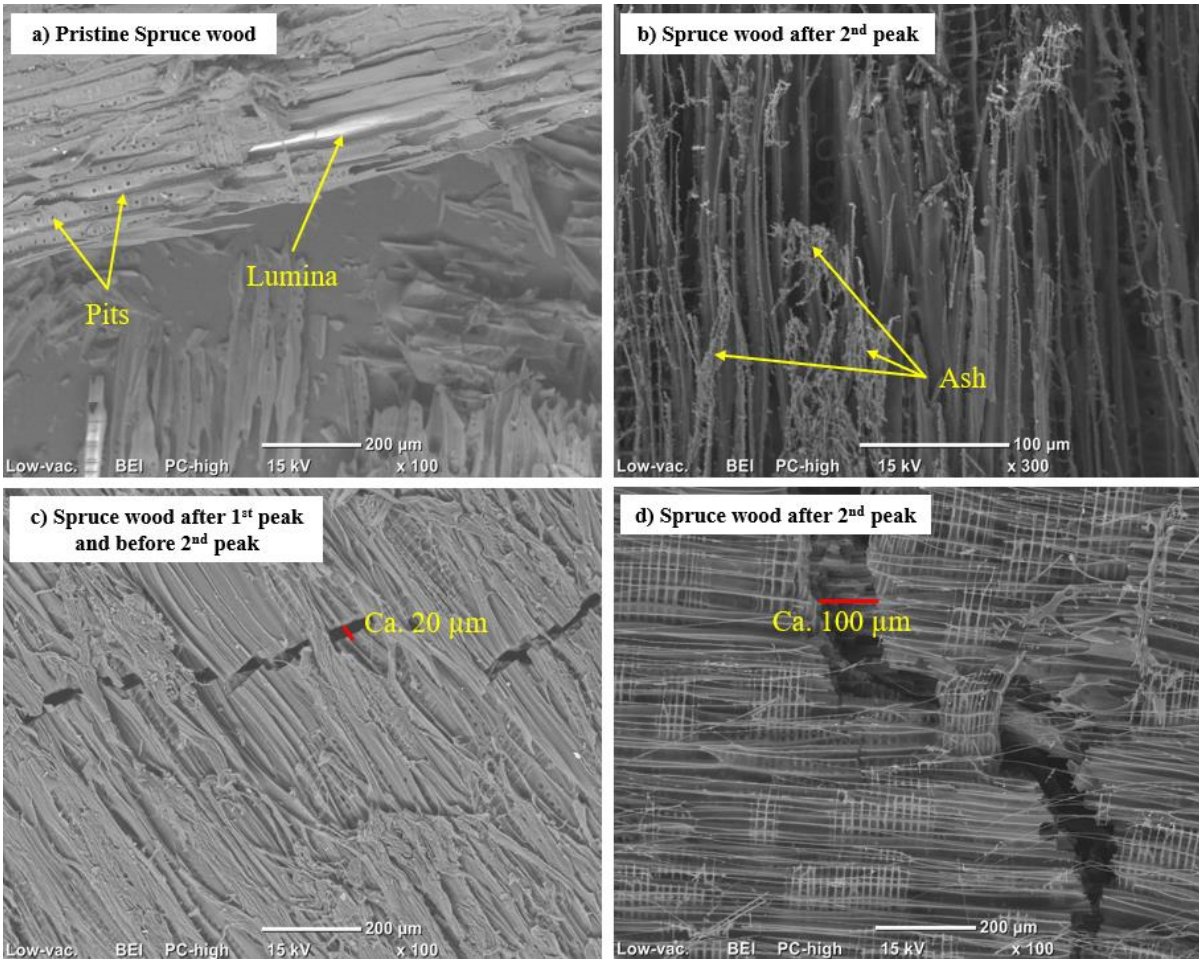

Figure 52. Images generated with SEM showing a) pristine spruce wood, b) wood with ash on the edge of the lumina after the second PHRR, c) crack in wood between the initial and second PHRR and d) crack in wood after the second PHRR.

5 Discussion and Analysis

The following section presents a discussion, analysis of the results, sources of error and suggestions for future work.

To gain a better understanding of the second peak in the HRR curve and to identify the cause of its appearance, multiple tests were performed with a cone calorimeter (heat flux of 35 kWm^{-2}) and SEM. Different rear materials, thicknesses and moisture content of spruce wood specimens were analysed to produce an in-depth analysis of the phenomena.

5.1 Heat release rate and temperature vs. rear material/substrate

Three types of materials were used on the rear side of the sample when mounted in the sample holder. These materials were kaowool, steel and aluminium foil wrapped around wood. The materials were chosen as their thermal properties are largely dissimilar. Kaowool provides little heat loss downwards in the sample holder and will instead facilitate heat accumulation, which raises the temperature and consequently increases the HRR. Steel has the opposite effect and works as a heat sink meaning it will conduct heat downwards. Aluminium foil wrapped around wood provides the same thermal properties as fresh wood where the only difference is that no further combustion will take place. Moreover, three different thickness of wood samples were analysed, i.e., 10, 20 and 30 mm. The different rear materials and sample thicknesses were used to identify and specify their effects on HRR.

Kaowool

Section 4.1.1 presents HRR and temperature tests with kaowool on the rear side of the sample. 10, 20 and 30 mm wood samples were analysed and the results can be seen in Figure 29. All samples experienced an initial peak with similar intensity occurring at the same time, thereafter the HRR rapidly decreased before rising again towards the second peak. Figure 31 shows pictures taken of different stages of the burning process. It is shown that the first peak is due to the ignition of the sample surface. It is also observed that char was forming on the surface right after the first peak, which worked as an insulating barrier and therefore decreased the HRR. All samples had similar initial peaks and decrease in HRR, the difference in HRR began when the HRR curves started to reach towards the second PHRR. Figure 29 shows that the 10 mm samples experienced the quickest and highest second PHRR of 160 kWm^{-2} whereas the slowest and lowest corresponding values were observed in the 30 mm samples of 78 kWm^{-2}. The difference in HRR between the samples was 82 kWm^{-2}, thus increasing the thickness by three times results in a reduction of almost half the second PHRR of the 10 mm sample. It is clear that an increased thickness results in a lower, broader and delayed second PHRR. This outcome is a response of the 30 mm samples taking longer to heat up compared to a thinner sample.

Figure 30 shows the temperature curves of the different samples. All samples reached similar maximum temperatures of 527-560 °C. The temperature kept rising after the second PHRR occurred. This indicated that the pyrolysis and char zone continued downwards through the specimen, which increased the temperature around the T/C the closer it got. Moreover, it was observed that a thicker wood specimen delayed the increase in temperature. A 10 mm sample experienced its maximum temperature around 650 s while a 20 and 30 mm sample reached their maximum temperature at 880 and 2340 s, respectively. Thus, increasing the thickness of a 10 mm sample to 20 and 30 mm resulted in an exponential time delay in temperature rise. All samples were analysed until flameout and Figure 322c-d shows that the samples have been

completely burnt by this time, meaning that when the rear side reaches around 530 °C the sample has no virgin wood left and what remains is only char and ash. This is supported by section 3.1.1 where it is mentioned that char is formed at 280-500 °C.

Steel plate

Section 4.1.2 presents HRR and temperature of samples with steel on the rear side. Samples of 10 mm were analysed together with 8 and 20 mm steel plates and 30 mm samples were tested with an 8 mm steel plate. Similar to the tests with kaowool the initial peaks in HRR, seen in Figure 33, occurred at the same time around 40-45 s with similar intensity. Different thicknesses of wood and steel were tested, it was observed that a second PHRR only appeared on the curve of the 10 mm wood samples with 8 mm steel plate on the rear side, with intensity of 83 kWm^{-2}. The 30 mm samples decreased in HRR after the initial peak due to char formation and continued with consistently low HRR until flameout. This was also seen for the 10 mm samples with a 20 mm steel plate where the only difference is that HRR decreased more rapidly, and flameout occurred at a much earlier stage than for both 10 and 30 mm wood with 8 mm steel.

Figure 35 shows the rear sides of all combinations of samples after flameout and cooldown. It is clearly seen that the sample that experienced a second PHRR (Figure 35a) is much more charred than the other two. There is only a little virgin wood left in the centre of the wood specimen. The other samples showed some charring on the corners of the rear side and the 10 mm sample with 20 mm steel showed the least amount of charring. Hence, the second PHRR is strongly dependent on the heat gradient reaching the back of the sample. When this happens the underlying material facilitates heat accumulation and pyrolysis gases will quickly escape and reach the flaming zone, which contributes with extra HRR. Steel, however, does not facilitate as much heat accumulation as kaowool resulting in a lower second PHRR. The reason why a second PHRR does not appear on the samples with less charring on the rear side is due to the conductive properties of steel. A thicker piece of steel will conduct the heat from the sample with better efficiency than a thin piece, and this reduces the heat available for combustion resulting in no second PHRR or charring on the sample backside.

The temperature curves of the samples are shown in Figure 34. The 10 mm sample with 8 mm steel reached the highest temperature of 429 °C on the rear side of the sample. 10 mm sample with 20 mm steel and 30 mm sample with 8 mm steel reached the lowest temperatures of 97 and 224 °C, respectively. The low temperature is an effect from the sample not being completely burnt before flameout, meaning that there is still virgin wood with a much lower temperature on the lower part of the sample where the T/C is located. According to section 3.1.1 the temperature needs to approach at least 280 °C for the wood to start charring.

Aluminium foil wrapped around wood

Section 4.1.3 introduces the results of the HRR and temperature tests with aluminium foil wrapped around wood. The results of HRR are consistent with that of kaowool and steel, see Figure 36. The initial PHRR was reached around the same time of 40-45 s. Thereafter, char formed leading to a decreased HRR. The 10 mm samples had the highest second PHRR of 122 kWm^{-2} and the 30 mm samples the lowest of 88 kWm^{-2}.

Figure 38 presents the backside of a 10 and 30 mm sample after flameout. Similar to the tests with kaowool, complete sample burn through was observed. The temperature of the rear side of the 10 and 30 mm samples experienced a maximum of 445 and 670 °C, respectively, see

Figure 37. As mentioned, char is formed around 280-500 °C, which explains why the residue is only char and ash.

5.1.1 Comparison between rear materials

A compilation of HRR and temperature for 10 and 30 mm samples with different rear material can be seen in section 4.1.4. It is observed in Figure 39 that all 10 mm samples reached the initial PHRR at the same time and had the same decrease rate when char formed. Moreover, the second PHRR occurred around the same time for all samples except for the samples with 20 mm steel plate. These samples did not experience a second peak, instead they had a constant decrease in HRR until flameout. The highest HRR was achieved by kaowool followed by aluminium foil wrapped around wood and 8 mm steel. This outcome was an effect from the thermal properties of the rear materials. Kaowool is an insulating material meaning that when heat approaches, it will prevent heat absorption and facilitate heat accumulation in the test specimen, which raises the temperature and HRR. Steel, however, is known for its conductive properties and heat will therefore travel through it. This resulted in a higher recorded HRR from samples with kaowool and a lower HRR from samples with steel.

Analysing the results of the 30 mm samples, Figure 41, it is seen that the samples with aluminium foil wrapped around wood had the highest second PHRR of 88 kWm^{-2} and not kaowool, which had a PHRR of 78 kWm^{-2}. From studying the results of the 10 mm samples kaowool is expected to have the higher PHRR, however, the difference of 10 kWm^{-2} is considered too small to be significant. The increase in HRR might be a response from combustion and escape of volatiles gases from the wood inside the aluminium foil.

Figure 40 presents the temperature curves of all 10 mm samples. Kaowool had the highest and quickest peak followed by aluminium foil wrapped around wood and 8 mm steel. The latter two reached roughly the same temperature with a difference of 16 °C. The biggest difference between the two is that steel delayed the time to reach this peak with around 200 s. This delay is a response of steel conducting the heat away from the sample making it more difficult for the temperature to rise. Temperature curves of the 30 mm samples are seen in Figure 42. The sample with aluminium foil wrapped around wood attained the highest temperature of 670 °C and kaowool had the second highest of 530 °C. This is most likely due to the same reason as mentioned in the paragraph above. If volatile gases escape and the wood inside the aluminium foil starts to combust it will increase both temperature and HRR.

5.2 Progression of char zone

Figure 47 and 48 show the progression of the char zone during the second PHRR of 10 and 20 mm samples with kaowool. A common denominator between the two is that during the rise of the second peak the char zone has reached the middle of the sample. It is also observed that at the top of the peak, the char zone has reached the rear side. Moreover, after the peak and close to flameout the samples are completely burnt.

10 mm samples with 8 mm steel were also analysed and Figure 49 shows the rear side of samples at various timesteps around the second PHRR. This sample combination was of particular interest since it was the only one of the different steel combinations that showed a second PHRR. Similar to the char progression of the 10 and 20 mm kaowool samples, it was seen that charring reached the backside of the sample and especially the corners. The appearance of a second PHRR is due to the rear material being thinner than e.g. a 20 mm steel plate, which understandably consists of more conductive material, thus a thicker plate conducts

heat more efficiently. Another parameter to consider may also be that the lid of the sample holder was not tight enough around the sample allowing easy air access by the corners of the lid. A 20 mm steel plate takes more space in the sample holder which tightens the wood to the lid. These findings support that the second PHRR is strongly affected by the heat gradient reaching the rear side.

5.3 Moisture transport

Samples with low moisture content (5-8 %) were analysed and the results is found in section 4.1.5. All samples experienced the initial PHRR around the same time followed by a decrease in HRR as char formed, see Figure 43. Similar to the analysed normal wood tests, it is the 10 mm samples that had the most rapid and highest second PHRR. However, a major disparity is seen in the 30 mm samples where a second and third HRR peak appeared, which is not observed in any other samples. Two out of three tested 30 mm samples showed three distinct peaks and no other thickness of the low moisture content samples experienced this phenomenon. Hence, more tests on 30 mm samples need to be tested in order to rule out the possibility that the occurrence of three peaks is only a coincidence and not a recurring pattern.

Comparing low moisture content samples and normal samples, see Figure 46, it is clear that a drier sample provides more intense HRR peaks, and less time is needed to reach flameout. It is mentioned in section 3.1.5 that upon heating, water starts to evaporate inside the wood. Some water vapour will leave through the sample surface, and some will migrate deeper into the material where it recondenses. Significant energy is required to undergo phase change leaving less energy accessible for pyrolysis. Therefore, fire spread rate is quicker in dry wood as all energy is used for pyrolysis.

Section 4.3 presents RH on the rear side of 10, 20 and 30 mm samples during analysis. As mentioned above, when the sample is exposed to heat, the water vapour moves deeper into the sample to recondense. This is supported by Figure 50 where it is shown that RH rose at the back of the sample during analysis. The samples were only analysed until the humidity probe reached 60 °C to avoid damage of the sensor, thus the entire burning process was not recorded.

The 10 mm sample had a fast humidity rise at the rear side as more water was pushed in that direction. The 20 and 30 mm samples had lower RH at the rear by the end of analysis. This is due to the wet zone (see Figure 20) having a larger volume when removed from the cone calorimeter, seen in Figure 51. Hence, the wet zone can therefore contain more moisture. However, it was observed that RH of the thicker samples decreased prior to removal from the cone calorimeter, therefore it cannot be determined if all thicknesses will reach the same level of humidity by the time of flameout.

5.4 Char microstructure

It is mentioned in section 3.2.3 that multiple and large holes in char structures enhance the exchange of volatiles and heat resulting in increased HRR. If the char is rigid and dense, volatiles are trapped and HRR is suppressed. In section 4.4 SEM images of pristine wood and char after the cone calorimeter tests are presented, seen in Figure 52. As the burning process proceeded and approached the second PHRR, cracks became increasingly distinct as the layer of char started to break down. After the second PHRR the cracks were at least three times wider, which is attributed to heating that is known to cause expansion. Wider cracks contribute to expansion of the surface area, which in turn facilitates increased burning. This implies that the formation of larger cracks and breakdown of char could contribute to increased HRR. However,

in section 5.1 it is observed that the time of the second PHRR was delayed with thicker samples. This refute char cracking as being a major reason for the time of occurrence of the second PHRR. Cracks form regardless of sample thickness and the peak should therefore have occurred earlier. Moreover, Figure 32a-b prove that cracks become wider and deeper when a sample is thicker, which means that HRR would increase as the surface area enlarges. This is, however, not observed in the cone calorimeter tests, a thinner sample experienced a more intense HRR than a thicker sample.

In conclusion, char cracking does not substantially contribute to the time of occurrence of the second PHRR but more so to the intensity of the overall HRR.

5.5 Appearance of HRR curve

The appearance of the HRR curve of wood can be explained and summarised into four parts, seen in Table 5.

Table 5. Summary of the points of interest in the HRR curve of wood.

Point of interest in HRR curve	**Explanation of appearance**
1st PHRR	At the start of the analysis the sample surface ignites causing significant production of heat, which in turn increases HRR, see Figure 31a. Normal spruce wood ignites around 25-40 s and dry spruce wood around 20-35 s. Thus, ignition time is roughly the same regardless of moisture content, sample thickness or rear side material. Ignition of the tested samples does not occur at one specific time. This may be due to a natural variation between the samples or by slight warping of the samples towards or away from the cone heater, which could either shorten or prolong the time to ignite. It could also be due to a difference in distance between the cone heater and samples. When a new sample thickness is introduced into the cone calorimeter the height of the scale needs to be adjusted by hand, which may result in a few millimetres height difference between samples.
Between 1st and 2nd PHRR	Between the two PHRR, the HRR decreases rapidly. This outcome is due to char formation on the surface of the sample. It is mentioned in section 3.1.2 that char works as a protective barrier that prevents mass transport of volatile gases and oxygen. Additionally, this is seen in Figure 31b.
2nd PHRR	Near the end of the tests, the HRR increases to a second peak. The PHRR becomes increasingly delayed with thicker samples and varies in intensity depending on the material beneath the wooden sample. This study has shown that the peak is a response to sample burn through, meaning that the heat gradient reaches the rear side of the sample. Kaowool, which is an insulator, hinders heat escape through conduction and facilitates heat accumulation, which raises the temperature of the entire sample consequently increasing the HRR and the second PHRR. Steel, however, is a heat sink, which will conduct heat away from the sample resulting in a lower PHRR. 10 and 30 mm wood with 20 and 8 mm steel, respectively, experienced no second PHRR. This outcome is due to the steel conducting too much heat to allow the wood sample to increase in burning, hence flameout occurred before the heat gradient reached the rear side of the sample.
After 2nd PHRR	After the second PHRR there is a distinct decrease in HRR as most of the fuel is now burnt. The sample is smouldering and expanding until the remaining flames die out, see Figure 31d.

5.6 Future work

This study was based on examining the appearance of the HRR curve of wood. By obtaining a deeper understanding, it is possible to improve the prediction of burning behaviour of wooden structures and determining the point at which the structural element is unstable.

It was seen that char has a great impact on the burning process and the overall HRR. Char acts as a protective barrier, which suppresses volatile gases and hence decreases HRR. It was, however, difficult to determine to what degree charring and char cracking affects the second PHRR. To study this phenomenon even further it would be interesting to use lasers to analyse the sample throughout the entire burning process. This would provide better understanding of the charring process, char cracking and in what way it affects the second PHRR.

A *Tinytag Plus 2 (TGP-4505)* was used to measure the moisture transport on the rear side of the samples during analysis. The humidity sensor did, however, have an operational temperature limit of 85 °C, consequently the entire burning process could not be recorded as the temperature eventually rose above this limit. To achieve better results of the moisture movement and its effect on HRR a humidity sensor that can endure higher temperatures would be required.

The HRR curves of 30 mm low moisture content wood showed both a second and third PHRR, which was not seen in any other sample. It would, therefore, be interesting to test additional samples of this size to further study the phenomenon and to observe if this was only a random incident that occurred for these three tested samples.

5.7 Source of error

The standard number of replications is three when using the cone calorimeter, therefore at least three replications were made of the different sample combinations. The degrees of freedom are, however, n-1 meaning that two samples are considered enough if it so happens that the results from one sample deviates from the others. Hence, enough samples were tested in this study to provide plausible results. The only argument to perform further tests would be to gain a better overview of the temperature curves. Almost all tested samples of the same sample composition presented different curves and therefore it was impossible to create a mean value-temperature curve. The reason for this outcome is most likely due to the temperature logger not recording properly, it is considered unlikely that samples of the same composition and similar HRR show such differences in temperature. A different temperature logger would be required in order to produce better results.

Moreover, when analysing the char progression of the second PHRR samples were removed from the cone calorimeter at certain sought-after stages to analyse the char microstructure and charring progression. However, since every HRR curve varied to some extent the time of removal was only a prediction from previous tests and thus causing a small uncertainty in the final result.

6 Conclusion

The purpose of this thesis is to provide an understanding of the HRR curve of wood when exposed to heating in the cone calorimeter. Fire development is often characterized in terms of HRR as a function of time. This makes HRR one of the most important variables in evaluation of material fire hazards. A better understanding of the burning process of wood enhances knowledge that can be used in both production and research.

Table 5 shows a thorough analysis of the burning process and HRR of wood when combusted in the cone calorimeter. The HRR curve of wood shows four major points of interest: the initial PHRR followed by a vast decrease in HRR, a second PHRR and finally a decrease in HRR until flameout. The initial PHRR is due to ignition of the sample surface, which causes intense production of heat that increases HRR. The ignition of the surface happens around 25-40 s for wood of normal moisture content (11.2-20.8 %) and around 20-35 s for low moisture content (5-8 %), thus ignition occurs around a similar time regardless of sample thickness or moisture content. The first decrease in HRR occurs when char begins to form on the surface. Char acts as a protective barrier, which prevents mass transport of oxygen and volatile gases, reducing the burning intensity and HRR. Close to the end of the burning process a second PHRR appears on the curve. This is due to sample burn through, i.e., when the heat gradient reaches the rear side of the wooden specimen. The intensity of the PHRR is heavily dependent on the type of rear material that is used. Kaowool is an insulator and thus hinders heat escape through conduction and facilitates more heat accumulation than, for example, steel, which is a conductor. The time of occurrence of the second PHRR is also delayed by high moisture content as a great amount of energy is required for water to undergo phase change. Therefore, wood containing a normal amount of water will reach the second PHRR at a later stage than dry wood as more water needs to evaporate. The last point of interest in the HRR curve is the final decrease in HRR, this occurs when most of the fuel is burnt leaving the sample to smoulder.

The formation of char does not have a significant impact on the second PHRR but more so to the overall HRR during combustion. Char has insulating properties, which obstruct the flow of oxygen and combustible gases that results in supressed burning and HRR.

6.1 Reflection

The purpose of this study was to gain deeper knowledge on the burning behaviour and HRR of wood, and moreover, to provide an understanding of the effects of char on HRR. The purpose of the study is considered fulfilled to the extent it was intended for. If the study were to be repeated, more tests need to be performed to be able to create a mean value of each temperature curve. Another option is to use a different temperature logger. Moreover, further tests need to be carried out on 30 mm low moisture content wood to identify if three peaks always appear on the HRR curve.

7 References

Bartlett, A. I., Hadden, R. M., & Bisby, L. A. (2019). A Review of Factors Affecting the Burning Behaviour of Wood for Application to Tall Timber Construction. In *Fire Technology* (Vol. 55, Issue 1). Springer New York LLC. https://doi.org/10.1007/s10694-018-0787-y

Björklund, M., & Paulsson, U. (2016). *Seminarieboken* (2nd ed.). Studentlitteratur.

Bogner, A., Jouneau, P. H., Thollet, G., Basset, D., & Gauthier, C. (2007). A history of scanning electron microscopy developments: Towards "wet-STEM" imaging. *Micron*, *38*(4), 390–401. https://doi.org/10.1016/j.micron.2006.06.008

Das, O., Kim, N. K., Hedenqvist, M. S., Bhattacharyya, D., Johansson, E., Xu, Q., & Holder, S. (2020). Naturally-occurring bromophenol to develop fire retardant gluten biopolymers. *Journal of Cleaner Production*, *243*. https://doi.org/10.1016/j.jclepro.2019.118552

Das, O., Kim, N. K., Hedenqvist, M. S., Lin, R. J. T., Sarmah, A. K., & Bhattacharyya, D. (2018). An Attempt to Find a Suitable Biomass for Biochar-Based Polypropylene Biocomposites. *Environmental Management*, *62*(2). https://doi.org/10.1007/s00267-018-1033-6

Das, O., Kim, N. K., Sarmah, A. K., & Bhattacharyya, D. (2017). Development of waste based biochar/wool hybrid biocomposites: Flammability characteristics and mechanical properties. *Journal of Cleaner Production*, *144*, 79–89. https://doi.org/10.1016/j.jclepro.2016.12.155

Fateh, T., Rogaume, T., Luche, J., Richard, F., & Jabouille, F. (2014). Characterization of the thermal decomposition of two kinds of plywood with a cone calorimeter - FTIR apparatus. *Journal of Analytical and Applied Pyrolysis*, *107*, 87–100. https://doi.org/10.1016/j.jaap.2014.02.008

Fire Testing Technology. (2009). *FTT Cone Calorimeter brochure*. http://www.fire-testing.com

FireSUN. (2021, September 21). *Cone Calorimeter & Heat Release Rates for Fire Engineering*. YouTube. https://www.youtube.com/watch?v=ztzvR8_mi8k&t=254s&ab_channel=FireSUN

Forest Products Laboratory. (2013). *Wood Handbook: Wood as an Engineering Material*. https://www.fpl.fs.fed.us/documnts/fplgtr/fpl_gtr190.pdf

Försth, M., & Roos, A. (2011). Absorptivity and its dependence on heat source temperature and degree of thermal breakdown. *Fire and Materials*, *35*(5), 285–301. https://doi.org/10.1002/fam.1053

Gan, W., Chen, C., Wang, Z., Song, J., Kuang, Y., He, S., Mi, R., Sunderland, P. B., & Hu, L. (2019). Dense, Self-Formed Char Layer Enables a Fire-Retardant Wood Structural Material. *Advanced Functional Materials*, *29*(14). https://doi.org/10.1002/adfm.201807444

Gemini Data Loggers. (n.d.). *Tinytag Plus 2 - TGP-4505*. Retrieved April 11, 2022, from https://www.geminidataloggers.com/data-loggers/tinytag-plus-2/tgp-4505

Hugget, C. (1980). Estimation of rate of heat release by means of oxygen consumption measurements. *Fire and Materials*, *4*(2), 61–65.

Jang, J., Lyu, H., Yang, H. J., Oh, M., & Lee, J. (2020). Deep learning-based autonomous scanning electron microscope. *IEEE International Conference on Intelligent Robots and Systems*, 2886–2893. https://doi.org/10.1109/IROS45743.2020.9341041

JEOL. (n.d.). *Scanning Electron Microscopes (SEM)*. Retrieved April 11, 2022, from https://www.jeol.co.jp/en/science/sem.html

Karlsson, B., & Quintiere, J. G. (2000). *Enclosure fire dynamics*. CRC Press.

Khatib, J. (2016). Sustainability of Construction Materials. *Woodhead Publishing*, *2nd revised edition*.

Kim, N. K., Bruna, F. G., Das, O., Hedenqvist, M. S., & Bhattacharyya, D. (2020). Fire-retardancy and mechanical performance of protein-based natural fibre-biopolymer composites. *Composites Part C: Open Access*, *1*. https://doi.org/10.1016/j.jcomc.2020.100011

Lindholm, J., Brink, A., & Hupa, M. (2009). *CONE CALORIMETER-A TOOL FOR MEASURING HEAT RELEASE RATE*. https://www.researchgate.net/publication/242266790

Lowden, L., & Hull, T. (2013). Flammability behaviour of wood and a review of the methods for its reduction. *Fire Science Reviews*, *2*(1), 4. https://doi.org/10.1186/2193-0414-2-4

L-Tube. (2021, June 23). *JEOL JCM-6000, Tabletop SEM*. YouTube. https://www.youtube.com/watch?v=N5NXRMrav6o&ab_channel=L-Tube

National Institute of Standards and Technology. (2021, December 3). *Cone Calorimeter*. https://www.nist.gov/laboratories/tools-instruments/cone-calorimeter

Puuinfo Ltd. (2020, July 31). *Moisture properties of wood*. https://puuinfo.fi/puuinfo-ltd/?lang=en

Schartel, B., & Hull, T. R. (2007). Development of fire-retarded materials - Interpretation of cone calorimeter data. *Fire and Materials*, *31*(5), 327–354. https://doi.org/10.1002/fam.949

Spearpoint, M. J., & Quintiere, J. G. (2001). Predicting the piloted ignition of wood in the cone calorimeter using an integral model - effect of species, grain orientation and heat flux. *Fire Safety Journal*, *36*, 391–415. https://www.sciencedirect.com/science/article/pii/S0379711200000552?via%3Dihub

Svenskt trä. (2016, December 29). *Brandegenskaper*. TräGuiden. https://www.traguiden.se/om-tra/materialet-tra/traets-egenskaper-och-kvalitet/termiska-egenskaper1/brandegenskaper/?previousState=000100

Svenskt trä. (2017, July 7). *7.1 Trä och brand*. TräGuiden. https://www.traguiden.se/konstruktion/kl-trakonstruktioner/kl-tra-och-brand/7.1-tra-och-brand/tra-och-brand/

Svenskt trä. (2020). *Om trä*. Träguiden. https://www.traguiden.se/om-tra/

Swapp, S. (n.d.). *Scanning Electron Microscopy (SEM)*. The Science Education Resource Center. Retrieved April 11, 2022, from https://serc.carleton.edu/research_education/geochemsheets/techniques/SEM.html

Swedish Wood. (n.d.). *Moisture content*. Retrieved April 12, 2022, from https://www.swedishwood.com/wood-facts/about-wood/wood-and-moisture/

Tran, H. C. (1992). (b) Experimental Data on Wood Materials. *Elsevier Applied Science*, 357–372. https://www.fpl.fs.fed.us/documnts/pdf1992/tran92a.pdf

Udoeyo, F. F., Inyang, H., Young, D. T., & Oparadu, E. E. (2006). Potential of Wood Waste Ash as an Additive in Concrete. *Journal of Materials in Civil Engineering*, *18*(4), 605–611. 10.1061/ASCE0899-1561200618:4605

Vaisala. (n.d.). *Relative Humidity - What Is It And Why Is It Important?* Retrieved April 11, 2022, from https://www.vaisala.com/en/blog/2018-10/relative-humidity-what-it-and-why-it-important

Wickström, U. (2016). *Temperature Calculation in Fire Safety Engineering* (1st ed.). Springer.

Appendix A – Kaowool

The following appendix present the recorded temperature of all tested samples with kaowool on the rear side. Figure 53, 54 and 55 show the temperature curves of 10, 20 and 30 mm samples respectively. Each sample thickness was tested three times. The samples had the same conditions and were exposed to a radiation of 35 kWm^{-2}.

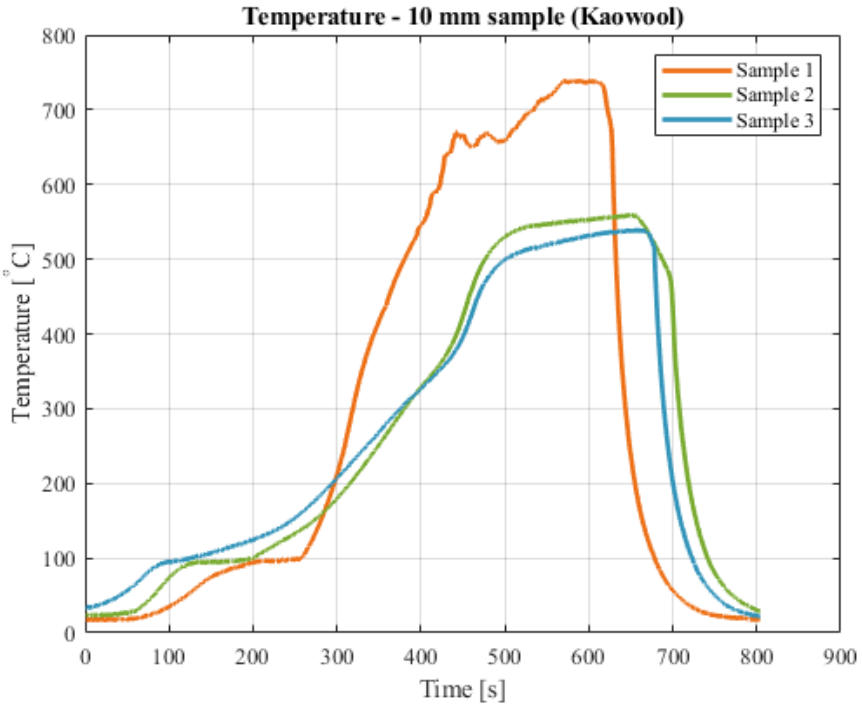

Figure 53. Temperature as a function of time for 10 mm wood samples with kaowool on the rear side.

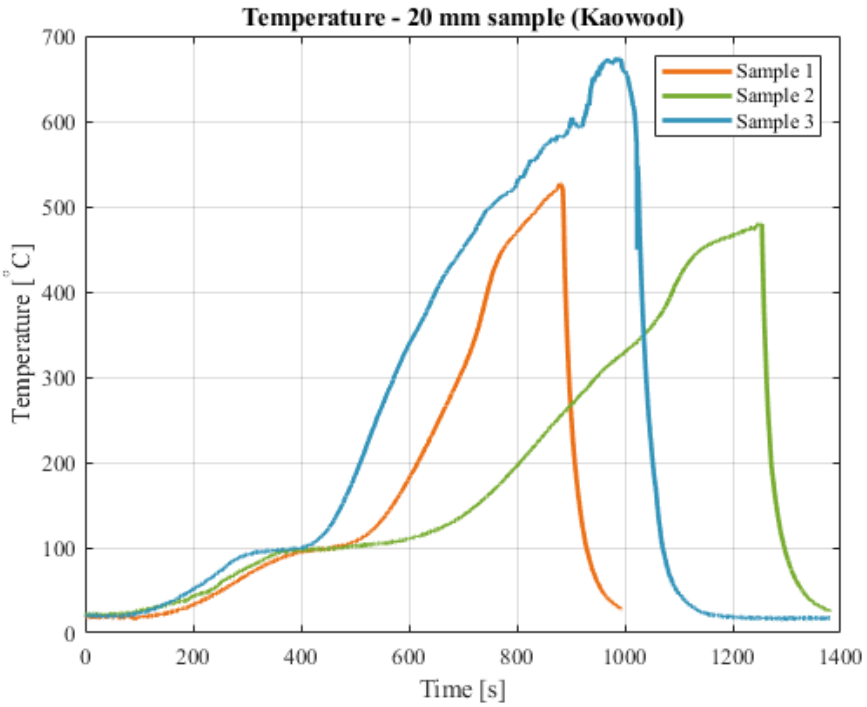

Figure 54. Temperature as a function of time for 20 mm wood samples with kaowool on the rear side.

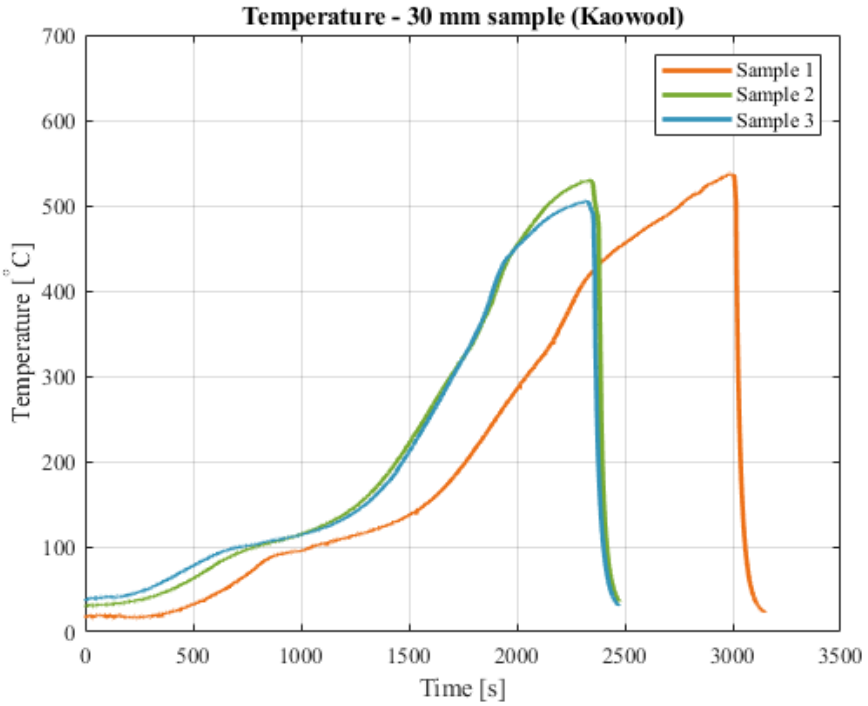

Figure 55. Temperature as a function of time for 30 mm wood samples with kaowool on the rear side.

Appendix B – Steel plate

The following appendix present the recorded temperature of all tested samples with a steel plate (8 or 20 mm) on the rear side. Figure 56, 57 and 58 show the temperature curves of 10 and 30 mm samples. Each sample and steel plate thickness were tested three times. The samples had the same conditions and were exposed to a radiation of 35 kWm^{-2}.

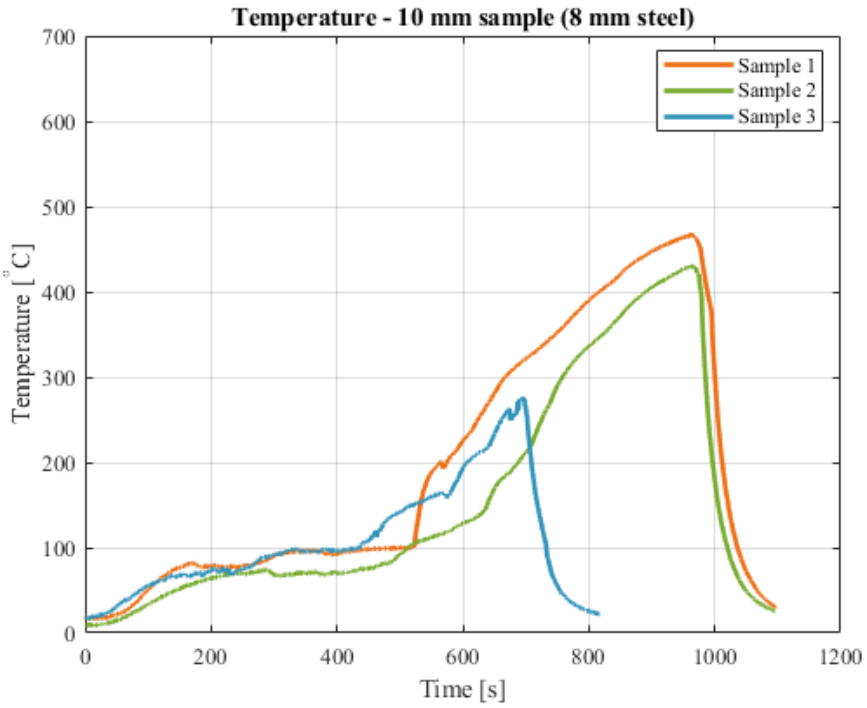

Figure 56. Temperature as a function of time for 10 mm wood samples with an 8 mm steel plate on the rear side.

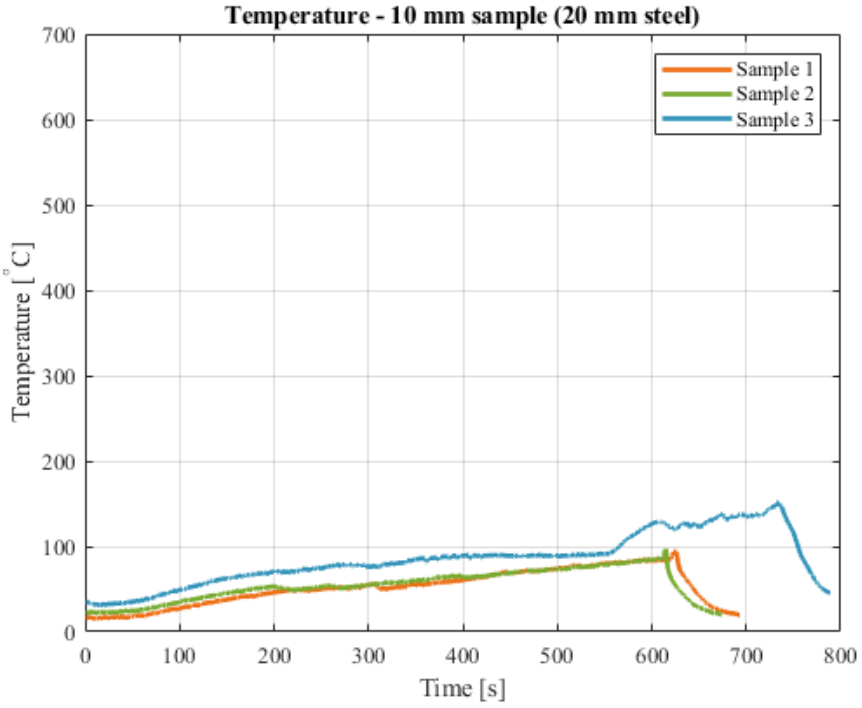

Figure 57. Temperature as a function of time for 20 mm wood samples with an 8 mm steel plate on the rear side.

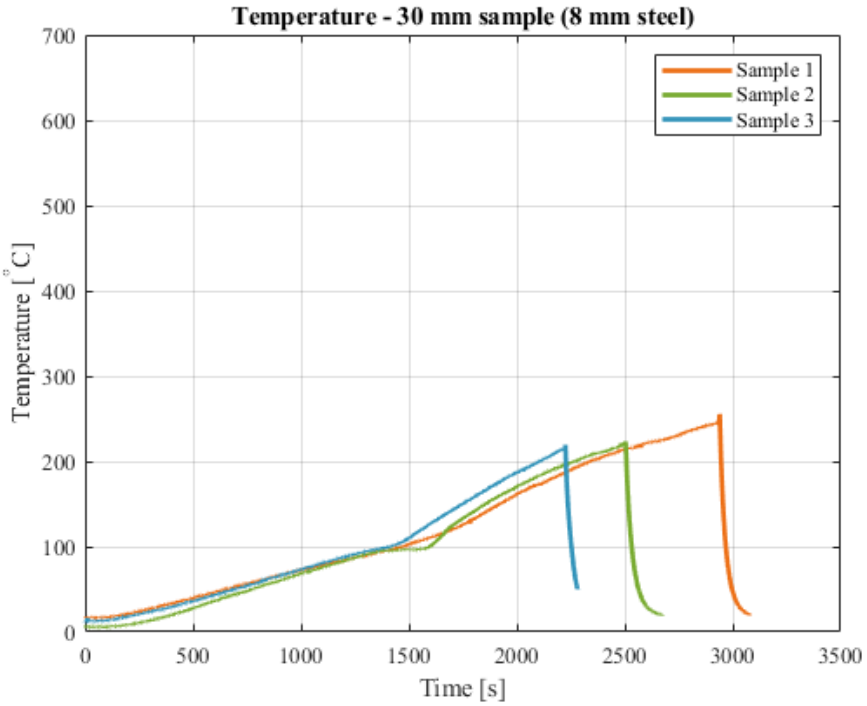

Figure 58. Temperature as a function of time for 30 mm wood samples with an 8 mm steel plate on the rear side.

Appendix C – Aluminium foil wrapped around wood

The following appendix present the recorded temperature of all tested samples with aluminium foil wrapped around wood on the rear side. Figure 59 and 60 show the temperature curves of 10 and 30 mm samples respectively. Each sample thickness was tested three times. The samples had the same conditions and were exposed to a radiation of 35 kWm^{-2}.

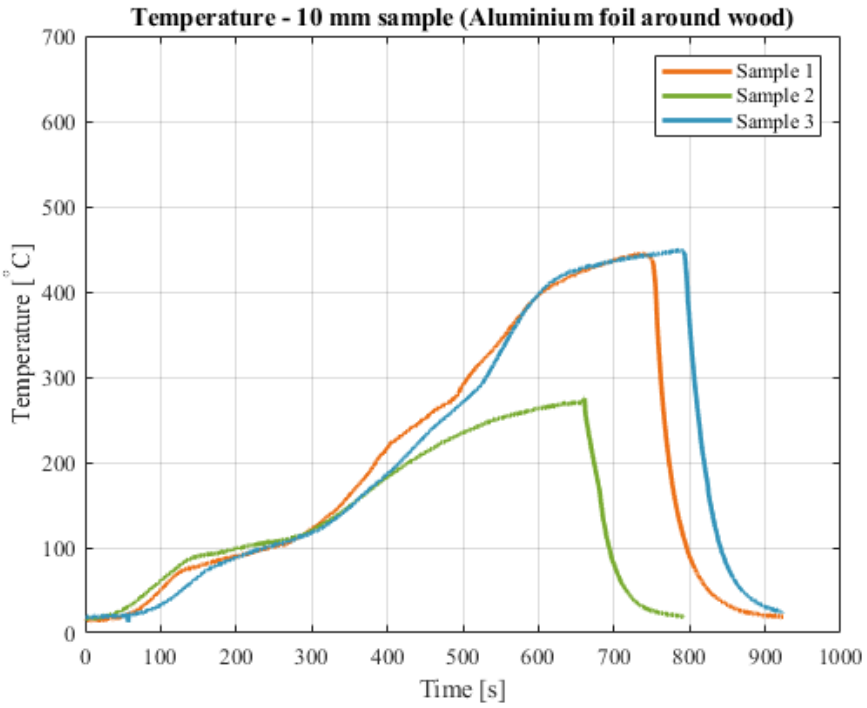

Figure 59. Temperature as a function of time for 10 mm wood samples with aluminium foil around wood on the rear side.

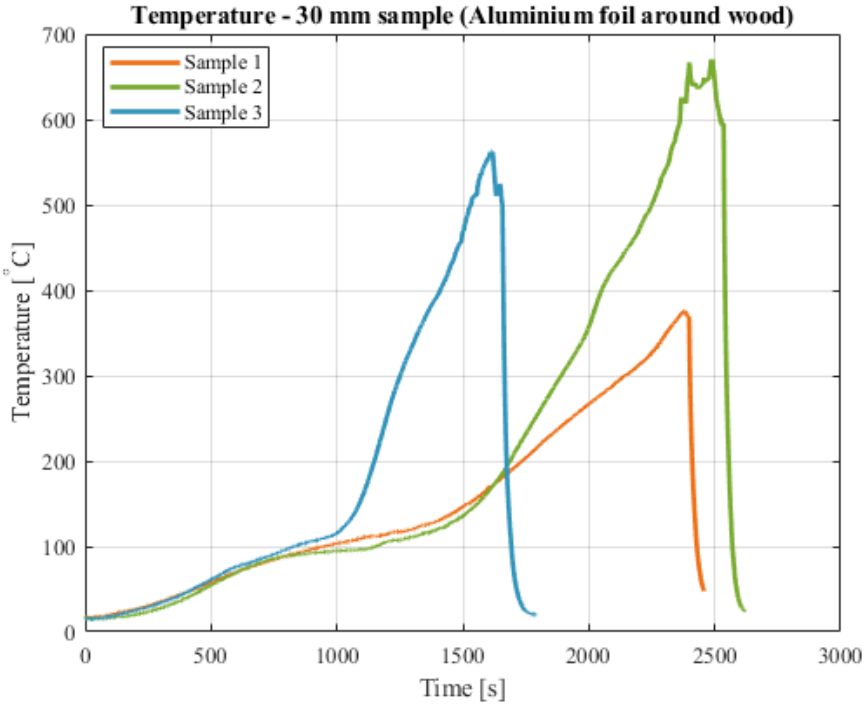

Figure 60. Temperature as a function of time for 30 mm wood samples with aluminium foil around wood on the rear side.

Appendix D – Low moisture content

The following appendix present the recorded temperature of all tested low moisture content (5 - 8 %) samples with kaowool on the rear side. Figure 61, 62 and 63 shows the temperature curves of 10, 20 and 30 mm samples respectively. Each sample thickness was tested three times. The samples had the same conditions and were exposed to a radiation of 35 kWm^{-2}.

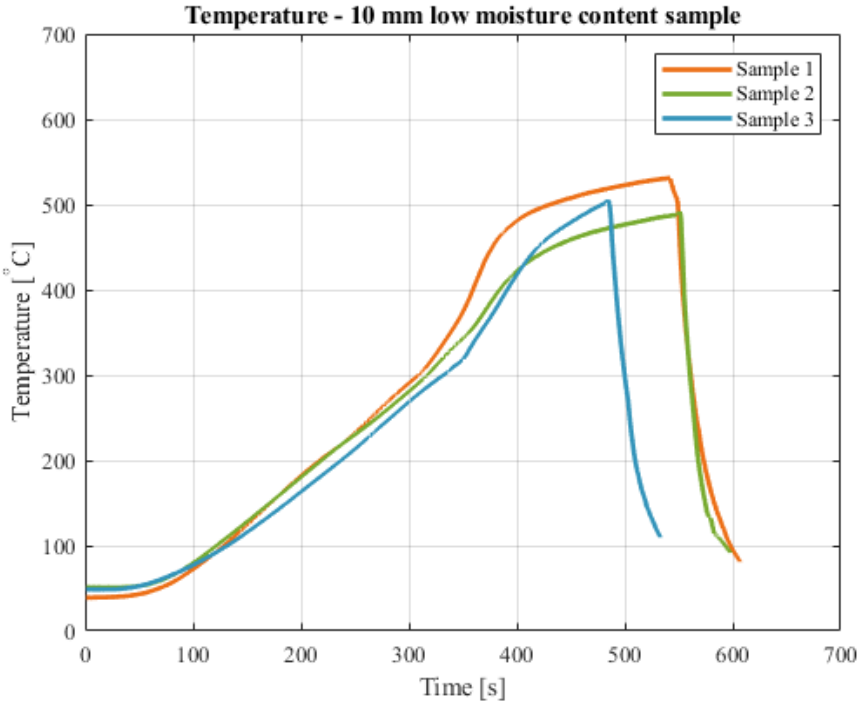

Figure 61. Temperature as a function of time for 10 mm low moisture content samples with kaowool on the rear side.

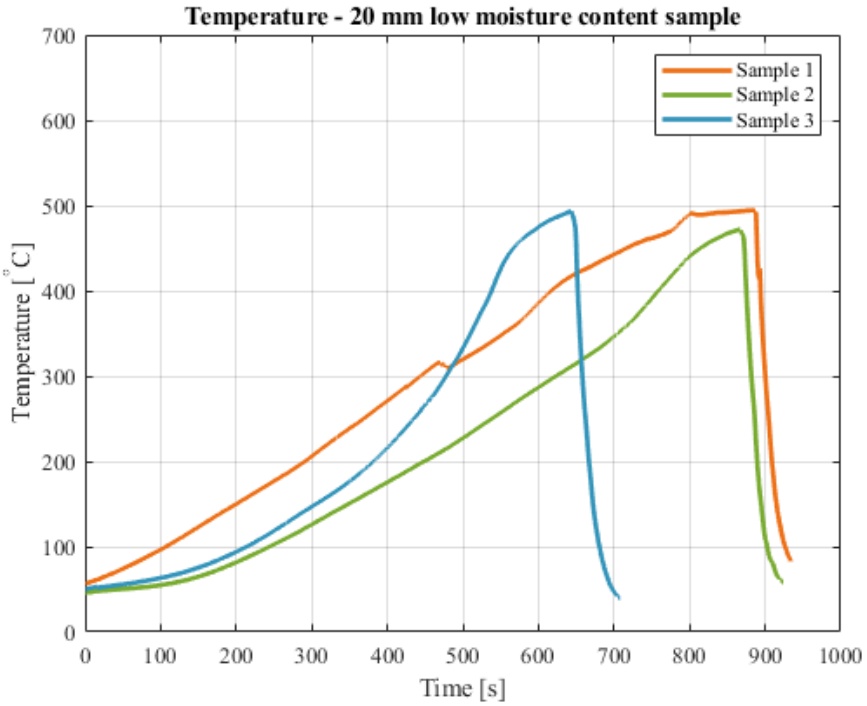

Figure 62. Temperature as a function of time for 20 mm low moisture content samples with kaowool on the rear side.

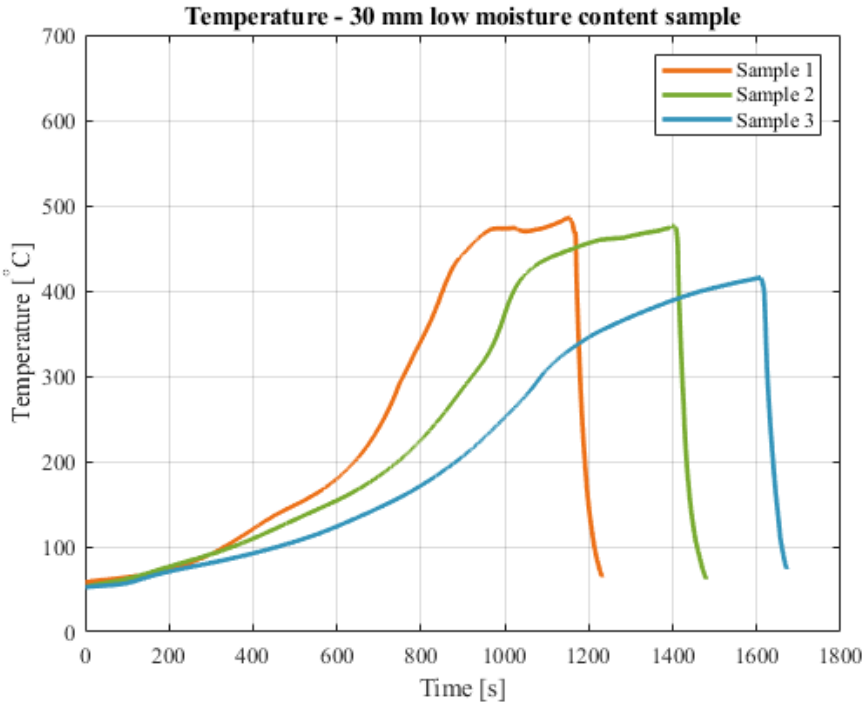

Figure 63. Temperature as a function of time for 30 mm low moisture content samples with kaowool on the rear side.